

Identifying and correcting interferences to PTR-ToF-MS measurements of isoprene and other urban volatile organic compounds

Matthew M. Coggon^{1*}, Chelsea E. Stockwell^{1,2}, Megan S. Claffin³, Eva Y. Pfannerstill⁴, Xu Lu^{1,2}, Jessica B. Gilman¹, Julia Marcantonio⁵, Cong Cao⁵, Kelvin Bates^{1,2}, Georgios I. Gkatzelis⁶, Aaron Lamplugh⁷, Erin F. Katz^{4,8}, Caleb Arata⁴, Eric C. Apel⁹, Rebecca S. Hornbook⁹, Felix Piel^{10,11,12}, Francesca Majluf^{3,a}, Donald R. Blake¹³, Armin Wisthaler^{10,11}, Manjula Canagaratna³, Brian M. Lerner³, Allen H. Goldstein^{4,14}, John E. Mak⁵, Carsten Warneke¹

¹NOAA Chemical Sciences Laboratory, Boulder, CO, 80305, USA

²Cooperative Institute for Research in Environmental Sciences, University of Colorado, Boulder, CO, 80305, USA

³Aerodyne Research, Inc., Billerica, MA, 01821, USA

⁴Department of Environmental Science, Policy, & Management, University of California Berkeley, Berkeley, CA, 94720, USA

⁵School of Marine and Atmospheric Science, Stony Brook University, Stony Brook, NY 11794, USA

⁶IEK-8: Troposphere, Forschungszentrum Jülich GmbH, Jülich, Germany

⁷Institute of Behavioral Science, University of Colorado, Boulder, CO, 80305, USA

⁸Department of Chemistry, University of California Berkeley, Berkeley, CA, 94720, USA

⁹Atmospheric Chemistry Observations & Modeling Laboratory, NCAR, Boulder, CO, 80301, USA

¹⁰Department of Chemistry, University of Oslo, Oslo, Norway

¹¹Institut für Ionenphysik und Angewandte Physik, Universität Innsbruck, Innsbruck, Austria

¹²IONICON Analytik GmbH, Innsbruck, Austria

¹³Department of Chemistry, University of California, Irvine, CA, 92697, USA

¹⁴Department of Civil and Environmental Engineering, University of California Berkeley, Berkeley, CA, 94720, USA

^aNow at Olin College of Engineering, Needham, MA, 02492

*Corresponding author: matthew.m.coggon@noaa.gov

Abstract: Proton-transfer-reaction time-of-flight mass spectrometry (PTR-ToF-MS) is a technique commonly used to measure ambient volatile organic compounds (VOCs) in urban, rural, and remote environments. PTR-ToF-MS is known to produce artifacts from ion fragmentation, which complicates the interpretation and quantification of key atmospheric VOCs. This study evaluates the extent to which fragmentation and other ionization processes impacts urban measurements of the PTR-ToF-MS ions typically assigned to isoprene (m/z 69, $C_5H_8H^+$), acetaldehyde (m/z 45, CH_3CHO^+), and benzene (m/z 79, $C_6H_6H^+$). Interferences from fragmentation are identified using gas chromatography (GC) pre-separation and the impact of these interferences are quantified using ground-based and airborne measurements in a number of

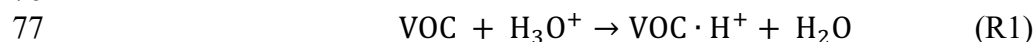
44 US cities, including Las Vegas, Los Angeles, New York City, and Detroit. In urban regions with
45 low biogenic isoprene emissions (e.g., Las Vegas), fragmentation from higher carbon aldehydes
46 and cycloalkanes emitted from anthropogenic sources may contribute to m/z 69 by as much as
47 50% during the day, while the majority of the signal at m/z 69 is attributed to fragmentation during
48 the night. Interferences are a higher fraction of m/z 69 during airborne studies, which likely results
49 from differences in the reactivity between isoprene and the interfering species along with the
50 subsequent changes to the VOC mixture at higher altitudes. For other PTR masses, including m/z
51 45 and m/z 79, interferences are observed due to fragmentation and O₂⁺ ionization of VOCs
52 typically used in solvents, which are becoming a more important source of anthropogenic VOCs
53 in urban areas. We present methods to correct these interferences, which provide better agreement
54 with GC measurements of isomer specific molecules. These observations show the utility of
55 deploying GC pre-separation for the interpretation PTR-ToF-MS spectra.

57 **1. Introduction**

58
59 Volatile organic compounds (VOCs) are an important contributor to urban air pollution. Once
60 emitted to the atmosphere, VOCs undergo chemical reactions that contribute to the formation of
61 hazardous pollutants such as ozone and secondary organic aerosol. It is important to quantify VOC
62 mixing ratios in urban areas to determine strategies that may reduce air pollution.

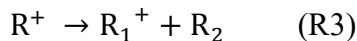
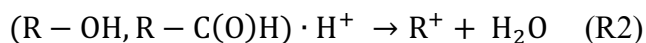
63
64 Proton-transfer-reaction time-of-flight mass spectrometry (PTR-ToF-MS) is a technique used to
65 measure a wide spectrum of VOCs, including oxygenates, aromatics, furanoids, nitriles, and
66 biogenic species such as isoprene and monoterpene isomers (Yuan et al., 2017). PTR-ToF-MS
67 measurements in urban regions enable the determination of VOC mixing ratios from an extensive
68 range of emission sources, including fossil fuels, solvent evaporation from volatile chemical
69 products (VCPs), residential wood burning, cooking, and urban foliage (Yuan et al., 2017). The
70 fast-time resolution and broad selectivity of PTR-ToF-MS measurements enables source
71 apportionment, flux estimates, and spatial mapping on mobile platforms that yield important
72 information about urban VOC source strengths (e.g., Gkatzelis et al., 2021a; Karl et al., 2018;
73 Pfannerstill et al., 2023b).

74
75 VOC detection by PTR-ToF-MS relies on analyte reactions with protonated water (Reaction 1).



77
78
79 Proton transfer is exothermic and spontaneous for VOCs with a proton affinity that is greater than
80 water. For many VOCs, including ketones, aromatics, and nitriles, the protonated product
81 (VOC · H⁺) is the primary signal detected by PTR-ToF-MS. For other VOCs, secondary reactions
82 including neutral loss of water, carbon fragmentation, and water clustering results in additional
83 product ions that can complicate the mass spectra. Pagonis et al. (2019) summarizes studies that
84 have reported fragmentation for a wide spectrum of species. Fragmentation is prevalent in
85 alcohols, aldehydes, and other species with long-chain alkane functionality (e.g., Buhr et al., 2002).
86 Small alcohols and aldehydes (C < 3) primarily react to form protonated products following R1,
87 while at higher carbon numbers, a large fraction of the reactions undergo neutral loss of water to
88 form a carbonium ion which may then undergo fragmentation to form lower-carbon ions (R2-R3).

89



93
94 R is the carbon backbone of an alcohol (R-OH) or aldehyde (RH=O), R⁺ is the product formed by
95 loss of water, R₁⁺ is a fragment, and R₂ is a neutral product. Fragmentation may also result from
96 protonation of cycloalkanes or alkyl aromatics. PTR-ToF-MS is not sensitive to small alkanes (C
97 < 5), but larger alkanes and cycloalkanes are detected at low sensitivity and upon ionization
98 subsequently fragment to produce ions that often overlap with the dehydration and fragmentation
99 products of alcohols and aldehydes (Arnold et al., 1998; Gueneron et al., 2015; Jobson et al., 2005).
100 The degree of dehydration and fragmentation is partially dependent on the strength of the drift
101 field (E) and density (N) (characterized by the E/N ratio), which impacts ion kinetic energy (Arnold
102 et al., 1998; Krechmer et al., 2018; Yuan et al., 2017; Holzinger et al., 2019). Lower E/N results
103 in lower fragmentation, but higher clustering with neutral water, which may further complicate the
104 mass spectra (Holzinger et al., 2019). Additional products may also be formed by reactions of
105 analytes with O₂⁺ and NO⁺ ions, which are present due to the ionization of small amounts of air in
106 the discharge reactor. The degree of ionization by these ions may vary depending on the ion source
107 design or relative humidity in the drift tube.

108
109 In the atmosphere, complex mixtures of emissions may result in PTR-ToF-MS mass spectra where
110 dehydration and fragmentation products interfere with the quantification of important atmospheric
111 VOCs. For example, PTR-ToF-MS measurements in regions with significant oil and natural gas
112 development show that substituted cycloalkanes fragment to produce significant signal at m/z 69
113 (C₅H₉⁺, Koss et al., 2017; Warneke et al., 2014; Pfannerstill et al., 2019). Likewise, interferences
114 have been observed downwind of urban and industrial environments (e.g., Inomata et al., 2010;
115 Choi et al., 2022). These fragments overlap with protonated isoprene and these previous studies
116 have shown that interferences make isoprene quantification challenging in these regions. In
117 forested areas, isoprene is largely emitted from biogenic sources and previous studies that have
118 compared PTR-ToF-MS measurements to those from gas-chromatography show good agreement
119 (e.g., Kaser et al., 2013). The impact of an interference to specific molecules, such as isoprene,
120 depends on atmospheric composition which changes spatially (e.g., urban vs. rural regions) and
121 temporally (e.g., summer vs. winter).

122
123 Assessments of interferences on PTR-MS measurements in urban atmospheres have been
124 conducted previously (e.g., Warneke et al., 2003), but the sources that contribute to urban VOCs
125 change on decadal timescales as fossil fuel emissions steadily decline (Kim et al., 2022; Warneke
126 et al., 2012). The urban atmospheric composition, once dominated by motor vehicle emissions, is
127 now composed of a higher proportion of oxygenates from solvents, other VOCs emitted from
128 sources such as volatile chemical products (VCPs), and cooking (Gkatzelis et al., 2021b;
129 McDonald et al., 2018a; Peng et al., 2022; Wernis et al., 2022). Significant advances in PTR-ToF-
130 MS detectors (quadrupole vs time-of-flight mass spectrometers) and drift tube designs have
131 enhanced instrument capabilities to acquire mass spectra with greater resolution and sensitivity
132 (Breitenlechner et al., 2017; Krechmer et al., 2018; Yuan et al., 2016; Holzinger et al., 2019).
133 These technological advances enable better identification and quantification and also an improved
134 understanding of the interferences that impact PTR-ToF-MS spectra.

136 With the changes in atmospheric composition and technological advances, it is necessary to revisit
137 potential interferences to commonly observed and reported VOCs by PTR-ToF-MS. In this study,
138 we investigate the interferences that impact PTR-ToF-MS spectra measured across several US
139 urban areas including Los Angeles, CA, Las Vegas, NV, Detroit, MI, and New York City, NY.
140 Interferences are identified using GC pre-separation, similar to previous measurements that
141 quantified PTR-ToF-MS fragmentation and interferences observed in complex mixtures, including
142 wildfire and urban emissions (e.g., Koss et al., 2018; Warneke et al., 2003). We show that
143 commonly measured species, such as acetaldehyde, benzene, and isoprene, exhibit interferences
144 from larger molecules associated with solvent use and cooking. The extent of these interferences
145 depends on the temporal and spatial variability of VOC emission sources. We present methods to
146 correct for these interferences based on the measurement capabilities of modern PTR-ToF-MS
147 instruments.

148

149 **2. Methods**

150

151 Table 1 summarizes the key field campaigns and instrumentation used to quantify VOCs and PTR-
152 ToF-MS interferences. Multiple PTR-ToF-MS instruments are used in this study and Table 1
153 outlines the PTR-ToF-MS reactor designs and drift tube operating parameters that play an
154 important role in determining ion distributions. The instruments described in this study use ion-
155 molecular reactors and ion optics devolved by Ionicon Analytik and TOFWERK, AG as described
156 by Müller et al. (2014) and Krechmer et al. (2018), respectively. In this study, all instruments were
157 operated with E/N 120 – 140 Td. The following sections describe each campaign and provide
158 additional details of instrument operation

159

160 **2.1.Campaign Descriptions**

161

162 **2.1.1. SUNVEx / RECAP-CA**

163

164 PTR-ToF-MS measurements were performed as part of the 2021 Southwest NO_x and VOC
165 Experiment (SUNVEx, <https://csl.noaa.gov/projects/sunvex/>) and Re-Evaluating the Chemistry of
166 Air Pollutants in California (RECAP-CA). SUNVEx was a ground campaign conducted to study
167 air quality in the Las Vegas Valley during the summer ozone season using both mobile and ground-
168 based sampling. The RECAP-CA campaign was conducted in Los Angeles and included mobile,
169 ground-based, and airborne sampling.

170

171 Measurements in Las Vegas were conducted between 30 June–27 July 2021 at an air quality
172 monitoring station located near the Jerome Mack Middle School (Fig. 1). Jerome Mack is an urban
173 background site located ~ 8km east of downtown Las Vegas. The site was chosen based on its
174 suite of trace gas and PM_{2.5} monitors and classification as a US Environmental Protection Agency
175 (EPA) Photochemical Assessment Monitoring Station (Annual Monitoring Network Plan, 2022).

176

177 **Table 1:** Summary of campaigns, instrumentation, drift tube operating parameters, and interferences reported for each campaign. Measurement uncertainties are
 178 for calibrated species reported in this study.

Region	Campaign	Sample Dates	Sampl. Strategy	Instrument Name	Type ^{1,2}	Reactor Design ³	Voltage	P (mbar)	T (°C)	E/N (Td)	Studied Interference
<i>Los Angeles</i>	RECAP-CA	Aug. 2 - 30, 2019	Ground	NOAA PTR-ToF-MS	TOFWERK	Vocus	650	2.5	110	140	m/z 69; m/z 79
	RECAP-CA	June 1 - 23, 2019	Airborne	Berkeley PTR-ToF-MS	TOFWERK	Vocus	590	2	60	130	m/z 69
	FIREX-AQ	Sept. 5, 2019	Airborne	Oslo PTR-ToF-MS	Ionicon	HC / DT	550	2.1	120	120	m/z 69
	FIREX-AQ	Sept. 5, 2019	Airborne	NOAA PTR-ToF-MS	TOFWERK	HC / DT	650	2.4	50	125	m/z 69
<i>Las Vegas</i>	SUNVEx	July 1 - 30, 2021	Ground / Mobile	NOAA PTR-ToF-MS	TOFWERK	Vocus	650	2.5	110	140	m/z 69; m/z 79; m/z 45
<i>Detroit</i>	MOOSE	May 21 - June 30, 2021	Ground / Mobile	Aerodyne PTR-ToF-MS	TOFWERK	Vocus	600	2.2	100	125	m/z 69; m/z 79
<i>New York City</i>	LISTOS	Jan. 2020 - April 2021	Ground	Stonybrook PTR-ToF-MS	Ionicon	HC / DT	600	2.3	60	130	m/z 69

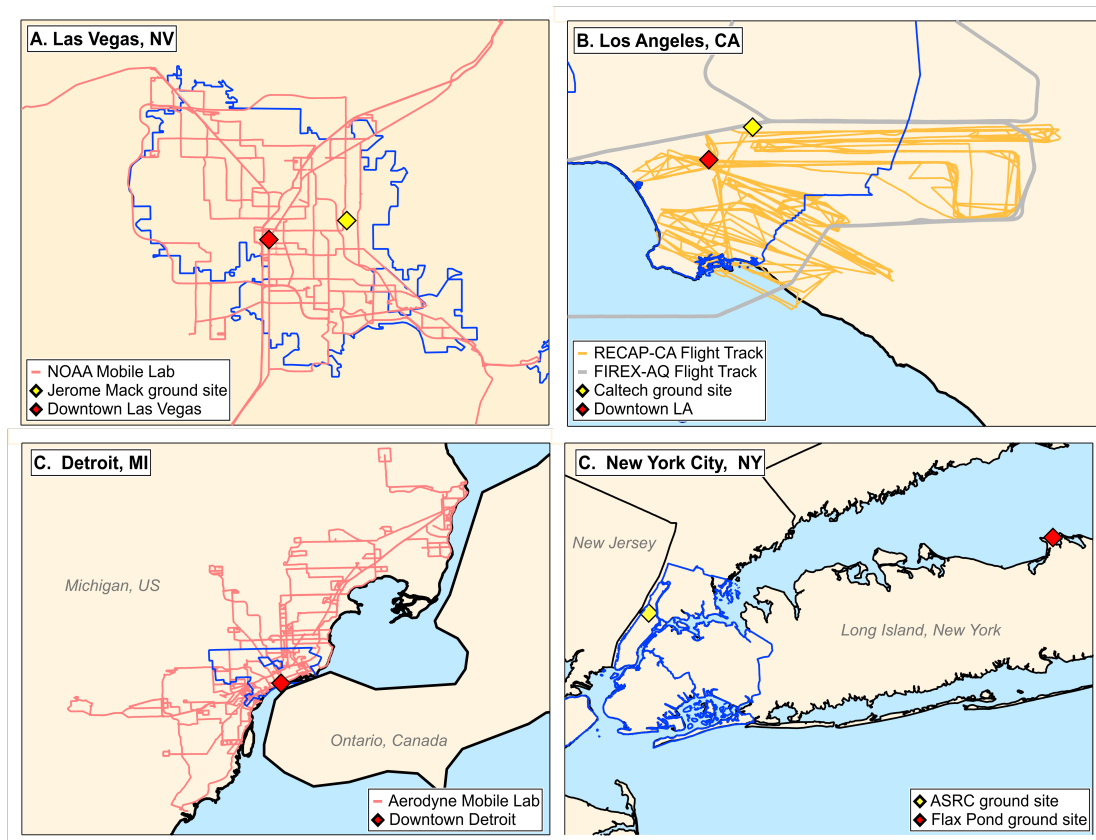
179 ¹ TOFWERK design PTR-ToF-MS using quadrupole ion optics as described by Krechmer et al. (2018).

180 ² Ionicon design PTR-ToF-MS with ion optics consisting of two einzel lens as described by Müller et al. (2014).

181 ³ HC / DT refers to the hollow cathode / drift tube design used in traditional PTR-MS instruments (e.g., Müller et al. 2014). The Vocus design is described by Krechmer et al. (2018).

183 Measurements in the Los Angeles Basin were conducted between 2 August and 5 September 2021
184 at the California Institute of Technology in Pasadena, CA (Caltech, Fig. 1). The ground site was
185 located within 0.5 km of the site used during the California Research at the Nexus of Air Quality
186 and Climate Change (CalNex) field study in order to directly compare with air quality
187 measurements conducted in 2010 (Ryerson et al., 2013). During this portion of the campaign,
188 instruments were situated in a trailer and sampled air from the top of a 10-m tower. The PTR-ToF-
189 MS sampled air with a bypass flow of $\sim 10 \text{ L min}^{-1}$ resulting in a residence time of $\sim 2 \text{ s}$. Long
190 sample lines may alter VOC distributions by acting as a sink, source, or reactive surface for various
191 compounds. These effects may contribute to the variability of interferences discussed here.

192 During both SUNVEx and RECAP-CA, the NOAA mobile laboratory was deployed to sample the
193 spatial distribution of VOCs and NO_x in regions of varying population density. A similar sampling
194 strategy was employed previously to study urban VOC enhancements in New York City and is
195 useful for identifying VOC signatures emitted from major sources, such as fossil fuels, VCPs, and
196 cooking activities (Coggon et al., 2021; Gkatzelis et al., 2021a; Gkatzelis et al., 2021b; Stockwell
197 et al., 2021). Drive tracks from the mobile laboratory are shown on the map in Fig. 1, along with
198 the locations of the ground sites and major population centers.



199
200 **Figure 1.** Mobile laboratory drive tracks, flight tracks, ground site locations, and locations of interest for the field
201 campaigns outlined in Table 1. The blue lines highlight the statistical metropolitan areas for Las Vegas, Los Angeles,
202 and Detroit, and the five boroughs of New York City.

203 The airborne component of RECAP-CA was conducted onboard the Naval Postgraduate School
204 UV-18A Twin Otter aircraft and was based out of an airport located in Burbank, CA.
205 Measurements of VOCs, NO_x, and greenhouse gases took place on nine days between 1 June and
206 23 June 2021. The Twin Otter typically flew at ~ 300 m above ground level at air speeds of 50 –
207 60 m s⁻¹. Each flight covered approximately 500 km of distance across the Los Angeles area,
208 including downtown, the coast, the Santa Ana area, and the San Bernardino Valley. The flight
209 track of the Twin Otter is shown in Fig. 1b.

210

211 **2.1.2. FIREX-AQ**

212

213 The 2019 Fire Influence on Regional to Global Environments and Air Quality (FIREX-AQ)
214 campaign was a large field study designed to investigate the emissions and atmospheric chemistry
215 of biomass burning emissions. A detailed description of the campaign, instrumentation, and
216 science goals is provided by Warneke et al. (2023). As part of the measurements, urban flights
217 were performed through the Los Angeles Basin on 5 September 2019. VOC measurements were
218 conducted onboard the NASA DC-8 by the NOAA PTR-ToF-MS and University of Oslo PTR-
219 ToF-MS. VOC measurements were also conducted by three GC instruments: the NOAA improved
220 Whole Air Sampler (iWAS), the University of California, Irvine Whole Air Sampler (WAS) and
221 the NCAR Trace Organic Gas Analyzer with a Time-of-Flight mass spectrometer (TOGA-TOF).
222 The flight tracks conducted in Los Angeles are shown in Fig. 1b.

223

224 **2.1.3. MOOSE Campaign**

225

226 The Michigan-Ontario Ozone Source Experiment (MOOSE) campaign was a multi-institutional
227 ground-based and mobile sampling effort conducted in 2021 to study ozone, meteorology, and
228 pollution in and around Michigan and Ontario. This region is currently designated as non-
229 attainment of the US federal ozone standard. Aerodyne Research, Inc. scientists deployed the
230 Aerodyne Mobile Laboratory (Herndon et al., 2005; Yacovitch et al., 2015) as part of the
231 CHEmical Source Signatures (CHESS) sub-experiment in order to measure emission plumes from
232 point sources and gain insight to the drivers of local ozone pollution during MOOSE. Other goals
233 of CHESS included developing emission source fingerprints for significant industrial source sites
234 in the area.

235

236 Ambient VOC measurements were conducted onboard the mobile laboratory using a PTR-TOF-
237 MS which was co-located with an *in situ* GC-EI-TOF-MS equipped with thermal desorption
238 preconcentration (Claflin et al., 2021). The AML sampled air around the Detroit metropolitan
239 region between 21 May and 30 June 2021 (Fig 1c). During mobile sampling, the mobile laboratory
240 transited through major population centers and targeted industrial point sources. Overnight and
241 when not driving, the mobile laboratory was stationed at the Salina Elementary/Intermediate
242 Schools in Dearborn, MI, parked at the Michigan Department of Environment, Great Lakes, and
243 Energy air monitoring station [AQS ID 26-163-0033].

244

245 **2.1.4. LISTOS**

246

247 The Stony Brook PTR-ToF-MS was deployed on the rooftop observatory at the Advanced
248 Sciences Research Center (ASRC) of the City University of New York to make continuous, high

249 time-resolution measurements of VOCs during the COVID lockdown from January 2020 to April
250 2021, (Fig. 1c; Cao et al., 2023). This campaign was a part of the broader Long Island Sound
251 Tropospheric Ozone Study (LISTOS). ASRC is located in the Manhattan Borough of New York
252 City, which is a highly urbanized region. Air was continuously sampled from a rooftop observatory
253 that is situated ~90 m above sea level on one of the tallest buildings in the vicinity of the site. In
254 June 2022, the Stony Brook PTR-ToF-MS was moved to the Flax Pond Marine Laboratory
255 (40°57'36"N, 73°8'24" W) near Stony Brook, New York, which is about 100 km east of ASRC
256 and located on the north side of Long Island in a forested suburban area. The Flax Pond Marine
257 Laboratory is a 0.6 km² preserve that encompasses a tidal wetland area and is operated for research
258 purposes by the School of Marine and Atmospheric Sciences of Stony Brook University. At Flax
259 Pond, air was continuously sampled from a ~10 m tower.

260

261 **2.2. Instrument Descriptions**

262

263 **2.2.1. NOAA PTR-ToF-MS**

264

265 The NOAA PTR-ToF-MS was deployed during SUNVEx, RECAP-CA, and FIREX-AQ. During
266 FIREX-AQ, the NOAA PTR-ToF-MS used a traditional ion source and drift tube as described by
267 Yuan et al. (2016). A full description of the operating parameters, VOC measurements, and
268 calibration methods are provided by Gkatzelis et al. (2022).

269

270 During SUNVEx and RECAP-CA, the instrument was modified to use the Vocus focusing ion
271 molecule reactor (TOFWERK, AG) and was operated following the recommendations by
272 Krechmer et al. (2018). The Vocus provides greater sensitivity to VOCs compared to the
273 traditional drift tube design due to the use of quadrupole ion guides that increase ion transmission.
274 Here, the Vocus was operated at 2.5 mbar and with an axial electric field gradient of 65 V cm⁻¹
275 (E/N ~ 140 Td). The water flow to the ion source was maintained at 23 mL min⁻¹ and the drift tube
276 was heated to 110°C. Typically, the quadrupole ion guide in the Vocus PTR-ToF-MS is operated
277 at voltages > 275 V to reduce the transmission of reagent ions that would otherwise limit the
278 lifetime of the detectors (Krechmer et al., 2018). Here, the quadrupole ion guide was tuned to 250
279 V to increase the transmission of ions produced from important VOCs with low molecular weights,
280 such as ethanol (m/z 47), acetonitrile (m/z 42), and methanol (m/z 33). Figure S1 compares the
281 product distribution of VOCs measured by the Vocus against those measured with the traditional
282 drift tube. In general, the ion product distributions are comparable, though small differences in
283 water clusters and fragmentation in the Vocus reflect the higher amount of water in the drift tube
284 and a higher operating E/N. The degree of fragmentation in the NOAA Vocus PTR-ToF-MS is
285 comparable to other PTR-MS systems with E/N > 120 Td (e.g., Buhr et al., 2002; Pagonis et al.,
286 2019). Other Vocus PTR-ToF-MS instruments used in this study observed higher fragmentation
287 owing to differences in operating conditions of the big-segmented quadrupole (BSQ). The
288 implications of fragmentation from the BSQ are discussed further in Section 3.1.

289

290 When installed on the mobile laboratory, the PTR-ToF-MS sampled air through a 1-m Teflon inlet
291 at 2 L min⁻¹, and instrument backgrounds were determined every 15 minutes. Instrument
292 backgrounds were determined hourly by passing ambient air through platinum catalyst heated to
293 350°C. The PTR-ToF-MS was calibrated using gravimetrically-prepared gas standards or by liquid
294 calibration (Coggon et al., 2018). Mixing ratios for calibrated species have uncertainties of ~ 20%.

295

296 **2.2.2. University of Oslo PTR-ToF-MS**

297

298 The University of Oslo PTR-ToF-MS was deployed during FIREX-AQ to target NH₃, but also
299 measured the same VOCs as the NOAA PTR-ToF-MS. The instrument was operated as described
300 by Müller et al. (2014) with modifications to reduce the formation of NH₄⁺ in the ion source as
301 described by Tomsche et al. (2023). Briefly, the instrument sampled air through a heated inlet at a
302 flowrate of 10–60 L min⁻¹ in order to reduce losses of NH₃ to inlet surfaces. The drift tube was
303 operated at 2.1 mbar and 120°C with corresponding E/N ratio of 120 Td. VOC sensitivities were
304 determined via calibrated using gravimetrically-prepared standards. Mixing ratios for calibrated
305 species have uncertainties of ~ 10% (Müller et al., 2014).

306

307 **2.2.3. University of California Berkeley PTR-ToF-MS**

308

309 The Berkeley Vocus PTR-ToF-MS (Aerodyne Research, Inc., Billerica, USA) was deployed
310 during the RECAP-CA aircraft campaign on the US Navy Twin Otter. The PTR-ToF-MS was
311 operated with a Vocus reactor set to 60°C, 2.0 mbar, and an E/N ratio of ~ 130 Td. The potential
312 gradient along the drift tube was 590 V. The gradient between BSQ skimmer 1 and skimmer 2 was
313 changed once during the campaign from 6 to 9.1 V, which resulted in an improved sensitivity for
314 some VOCs, but significantly stronger fragmentation for other compounds such as nonanal (Fig.
315 S2). Both operating conditions were calibrated. The reagent water flow was 20 mL min⁻¹. Similar
316 to the NOAA-PTR-ToF-MS, the voltage of the quadrupole ion guide was operated at 200 V to
317 improve the transmission for low-mass VOCs like methanol.

318

319 Ambient air was sampled via a 90 cm long heated (40°C) ¼-inch Teflon line through a Teflon
320 filter from an isokinetic inlet (flow rate ~ 6 m s⁻¹ for 5 m length) with a mass flow controller at 1.5
321 L min⁻¹. Mass spectra were recorded at 10 Hz time resolution for a mass range of 10-500 Da. Zero-
322 air blank measurements were conducted several times in each flight for 1-5 minutes during aircraft
323 turns ~ 2-4 times per flight, each followed by a pulse of calibration gas ~ 1-5 minutes in duration.
324 These in-flight calibrations were used to validate the sensitivities calculated from ground
325 calibrations. Ground calibrations were conducted every 1-3 days (in total, 19 times) during the
326 campaign using one of three gravimetrically prepared multicomponent VOC standards (Apel-
327 Riemer Environmental Inc., Miami, FL, USA). More details on the instrument operation,
328 calibration, and determination of uncertainties can be found in Pfannerstill et al. (2023b). Mixing
329 ratios for calibrated species have uncertainties of ~ 20%.

330

331 **2.2.4. Aerodyne PTR-ToF-MS**

332

333 Aerodyne Research, Inc. deployed a Vocus PTR-ToF-MS during MOOSE 2021 (Krechmer et al.,
334 2018; Riva et al., 2019). The Vocus was operated at a pressure of 2.2 mbar and axial voltage
335 gradient of 600 V, corresponding to an E/N ratio of 125 Td. Data were recorded and processed at
336 1 Hz time resolution using the Tofware software (Aerodyne Research Inc. and TOFWERK) in
337 Igor Pro (WaveMetrics) (Stark et al., 2015). Background measurements were conducted every 16
338 minutes by overflowing the Vocus inlet with air from a zero-air generator (ZAG) equipped with a
339 Pt/Pd catalyst at 400°C. Calibrations were performed every 4 hours with a multicomponent VOC

340 mixture (Apel-Riemer Environmental Inc., Miami, FL, USA; nominal 1 ppm in N₂) diluted with
341 ZAG air. Mixing ratios for calibrated species have uncertainties of ~ 20% (Krechmer et al., 2018).

342

343 **2.2.5. Stony Brook PTR-ToF-MS**

344

345 The Stony Brook Ionicon high-resolution PTR-ToF-MS (Ionicon 8000, Analytik GmbH, Austria)
346 was deployed in New York City during the COVID shutdown, and subsequently at Flax Pond on
347 Long Island. In this study, the Stony Brook PTR-ToF-MS was operated with a drift field of ~130
348 Td, drift voltage of 600 V, reactor temperature of 60°C, and drift tube pressure of 2.3 mbar. The
349 instrument sampled VOCs through a heated (60°C) 1/16-inch outer diameter (O.D.) capillary
350 PEEK inlet (~1 m length) with bypass flow line teed off the 1/2-inch PTFE inlet line fitted with a
351 blower on the back end (residence time of the gas was ~10 s). Data were collected at 1 Hz and
352 integrated to 5-minute averages.

353 Calibrations were performed using a dynamic dilution system. VOC-free air was produced by
354 pumping ambient air through a Pt-based catalytic converter at 400°C, then mixed with
355 multicomponent gas calibration mixture (Apel-Riemer Environmental Inc., Miami, FL, USA) that
356 included isoprene. Calibration was performed spanning a concentration range of observed values
357 (0, 5, 10, 15, 20 ppbv). At ASRC, the calibration gas was typically analyzed twice a week prior to
358 the COVID-19 lockdown, and typically every 1-2 weeks during the lockdown given limited access
359 to the observatory. At Flax Pond, the calibration gas was analyzed once a week. Mixing ratios for
360 calibrated species have uncertainties of ~ 20% (Cao et al., 2023)

361

362 **2.2.6. GC-PTR-ToF-MS and other GC-MS instruments**

363

364 To guide the identification of the proton-transfer-reaction products, a GC was used to trap and pre-
365 separate ambient VOCs sampled by the NOAA PTR-ToF-MS during SUNVEx. The GC deployed
366 here is the same instrument used by Stockwell et al. (2021) to identify molecular isomers measured
367 from coating headspaces. Briefly, the GC consists of a liquid nitrogen cryotrap coupled to a DB-
368 624 column (Restek MXT-624; 30-m length × 0.25-mm inner diameter (I.D.), 1.4-µm film
369 thickness). Samples were collected onto the cryotrap at predetermined volumes (typically 80 cm³),
370 then injected onto the column via rapid heating to 100°C. Nitrogen gas carried the sample through
371 the column at 8 sccm while the column was heated from 40°C to 150°C at a rate of 12°C min⁻¹.
372 The effluent from the column was injected into the PTR-ToF-MS inlet. In this study, we use this
373 setup (termed GC-PTR-ToF-MS) to qualitatively assess isomer distributions and fragmentation
374 patterns for VOCs detected during *in situ* sampling.

375

376 The GC-PTR-ToF-MS was primarily deployed during the ground-based sampling phase in Las
377 Vegas. Samples were collected every 2 hours and automatically analyzed by PTR-ToF-MS. In
378 between GC measurements, the PTR-ToF-MS sampled ambient air through a 10-m Teflon inlet at
379 2 L min⁻¹. During an evening drive on 31 July 2021, the GC-PTR-ToF-MS was deployed to
380 speciate VOCs on the Las Vegas Strip, where large crowds of people were present and
381 anthropogenic emissions from personal care products, cooking, and other human activities were
382 expected to be highest.

383

384 Additional GC measurements were conducted as part of the field campaigns described in Section
385 2.1. A full description of these measurements are described in the Supplemental Information.

386
387
388
389
390
391
392
393
394
395
396
397
398
399
400
401
402
403
404
405
406
407
408
409
410
411
412
413
414
415
416
417
418
419
420
421
422
423
424
425
426
427
428
429
430
431

3. Results

The following sections outline PTR-ToF-MS interferences observed for ions typically assigned to isoprene, oxygenated VOCs, and aromatic VOCs. The primary data used for this analysis are from the NOAA PTR-ToF-MS, which provided direct evidence of interferences via GC pre-separation. Each section begins with a description of GC-PTR-ToF-MS samples collected along the Las Vegas Strip during SUNVEx. This region comprises many hotels and entertainment establishments and is impacted by emissions from fossil fuels, VCPs, and restaurant cooking. This region had the highest observed mixing ratios compared to New York, Detroit, and Los Angeles. These interferences are then compared to ground site data collected by the NOAA PTR-ToF-MS during SUNVEx/RECAP-CA. Finally, observations from other instruments in cities across the US are presented to show the ubiquity of these interferences across instruments and urban environments. Where possible, we describe methods to correct for interferences.

A key focus of this discussion is the impact of fragmentation on PTR-ToF-MS observations of the $C_5H_8H^+$ ion at m/z 69.070 (henceforth referred to as “ m/z 69”). This ion is typically assigned to isoprene and mixing ratios are determined based on measurements of isoprene standards; however, the raw signals at this mass may include contributions of other compounds due to fragmentation. Throughout the discussion, we report m/z 69 mixing ratios calculated using PTR-ToF-MS sensitivities towards isoprene in order to demonstrate the extent to which interferences bias estimations of isoprene mixing ratios. We note that this analysis only reflects interferences attributable to high-resolution PTR-MS systems. Quadrupole or compact time-of-flight mass spectrometers measure additional ions that are isobaric to $C_5H_8H^+$ (e.g., furan, $C_4H_4OH^+$ at m/z 69.034) and further corrections are needed to these data to resolve isoprene mixing ratios.

3.1. Isoprene

3.1.1. Known interferences to isoprene (m/z 69)

Biogenic VOCs are commonly reported by PTR-ToF-MS, including isoprene and the sum of monoterpene isomers. Isoprene is the dominant biogenic VOC emitted by urban foliage and is a major contributor to urban OH reactivity (Calfapietra et al., 2013). Interferences to isoprene in PTR-ToF-MS spectra result from the production of the $C_5H_8H^+$ ion, which is a common fragment for higher-carbon aldehydes ($> C_5$), alkenes, and cycloalkanes (Buhr et al., 2002; Gueneron et al., 2015; Pagonis et al., 2019; Romano and Hanna, 2018). Previous studies have characterized ambient isoprene interferences from 2-methyl-3-buten-2-olalkenes emitted from biogenic sources (e.g., Karl et al., 2012) and cycloalkanes emitted from fossil fuels use and oil and natural gas production (e.g., Gueneron et al., 2015; Warneke et al., 2014; Pfannerstill et al., 2023b). For example, Gueneron et al. (2015) showed that substituted cyclohexanes and cyclohexenes produce fragmentation patterns that consist largely of m/z 111, m/z 125, m/z 69, m/z 83, m/z 57, and other lesser-abundant hydrocarbon fragments. In regions with significant oil and natural gas development, these compounds may produce interferences at m/z 69 which can interfere with the signal resulting from biogenic sources of isoprene (e.g., Warneke et al., 2014). Similarly, Kilgour et al. (2021) show that aldehydes emitted due to ozone deposition to surface ocean waters may interfere with the quantification of isoprene. The key aldehydes observed to produce an

432 interference were nonanal and octanal. The same aldehydes may be produced on inlet surfaces
433 exposed to high ozone concentrations and result in an isoprene artifact (Ernle et al., 2023;
434 Vermeuel et al., 2022).

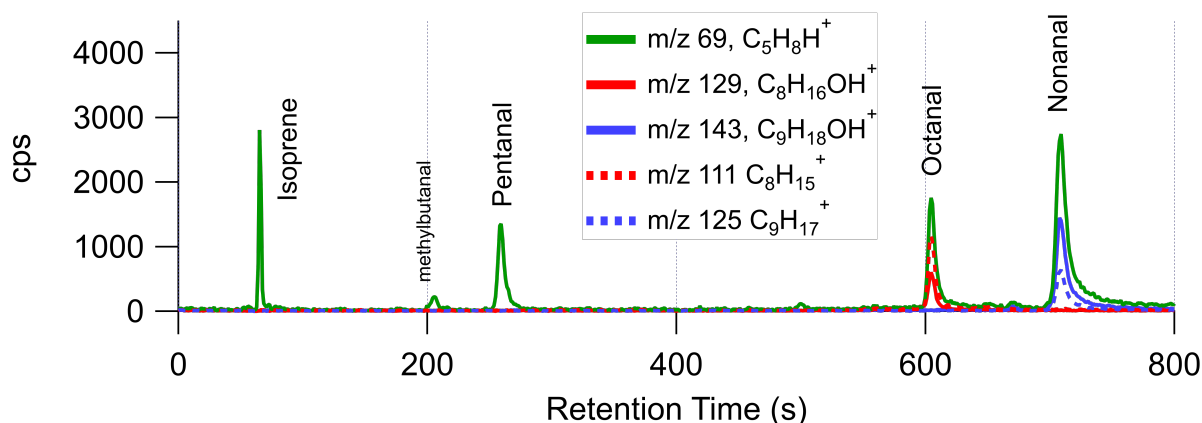
435
436

3.1.2. Characterizing aldehyde interferences to m/z 69 using GC-PTR-ToF-MS

437
438

439 Figure 2 shows a GC-PTR-ToF-MS chromatogram of the ion typically assigned to isoprene (m/z
440 69, $C_5H_8H^+$). This sample was collected on the Las Vegas Strip in the evening (~ 22:15 local time,
441 LT) when biogenic emissions of isoprene are expected to be low. The chromatogram shows that
442 isoprene (retention time, RT = 65 s) is only a small contributor to the signal at m/z 69 measured in
443 this region. Additional peaks are observed at RT = 210 s, 250 s, 600 s, and 710s. These peaks are
444 not cycloalkanes, as might be expected from mobile source emissions (Gueneron et al., 2015);
445 rather, these are fragmentation products of saturated aldehydes, including methylbutanal, pentanal,
446 octanal, and nonanal. Chromatograms of the parent ions attributed to octanal and octanone (m/z
447 129, $C_8H_{16}OH^+$), together with nonanal and nonanone (m/z 143, $C_9H_{18}OH^+$) are shown in Fig. S3.
448 The parent ion and the water-loss products (m/z 111 $C_8H_{15}^+$ and m/z 125 $C_9H_{17}^+$, respectively) are
449 observed, but at different ratios between the aldehydes and ketones. Pentanal and methylbutanal
450 almost entirely fragment and do not exhibit significant signal at the parent ion mass. Comparisons
451 of ambient observations with GC-PTR-ToF-MS chromatograms of standard mixtures show that
452 only aldehydes (and not the ketones) are observed in significant quantities on the Las Vegas Strip
453 (Fig. S3).

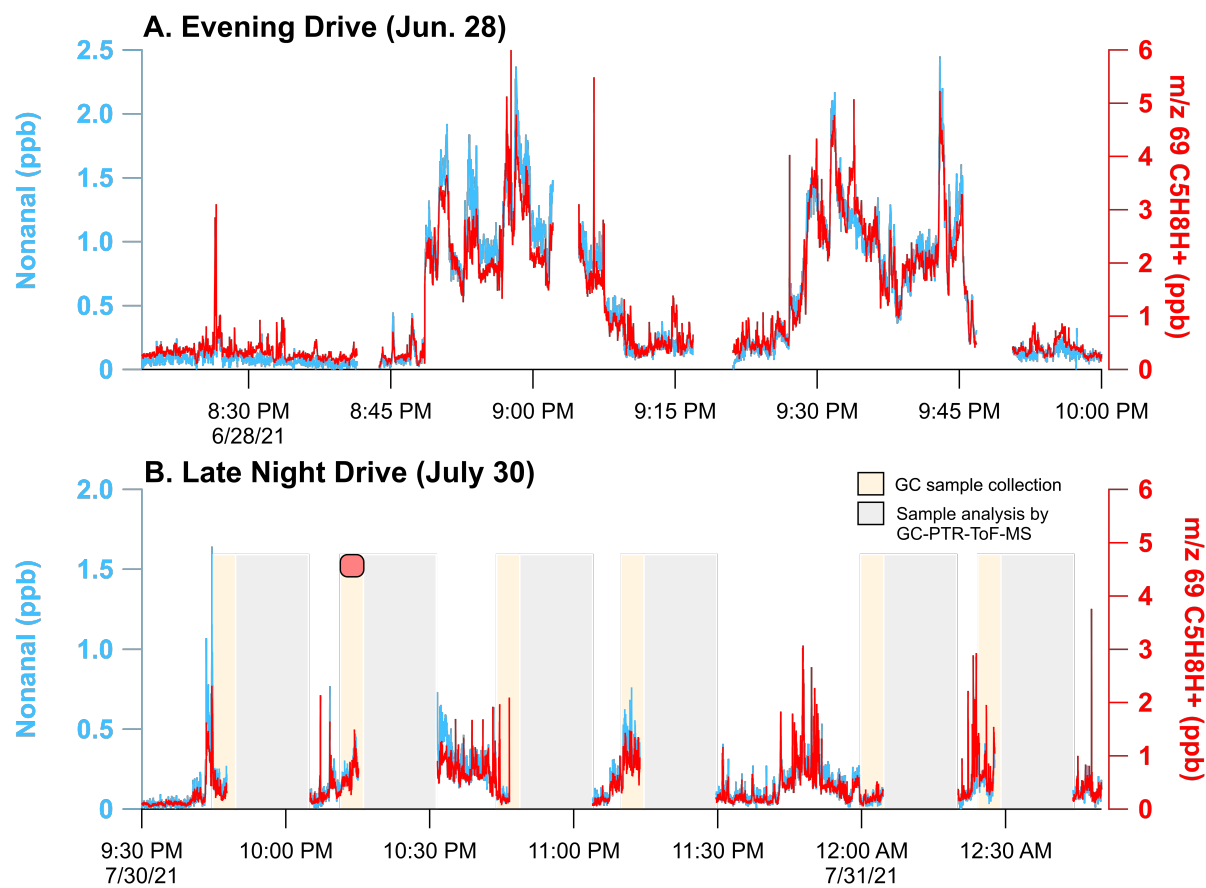
454
455
456



457
458 **Figure 2.** GC-PTR-ToF-MS chromatogram from downtown Las Vegas at 22:15 on 30 July 2021, showing the
459 contributions of isomers and fragments to the ion typically assigned to isoprene (m/z 69, $C_5H_8H^+$).
460

461 These aldehydes emissions likely result from cooking (Arata et al., 2021; Klein et al., 2016;
462 Schauer et al., 1999; Karl et al., 2018; Wernis et al., 2022) and their significant presence on the
463 Las Vegas Strip possibly reflects the high density of restaurants along Las Vegas Boulevard.
464 Figure 3 shows mobile laboratory measurements of nonanal and m/z 69 during evening drives on
465 28 June and 30 July 2021. GC-PTR-ToF-MS sampling was only conducted on 30 July and the
466 location of the sample (Las Vegas Strip) is shown in Fig. 1a. During both drives, m/z 69 was

467 enhanced along Las Vegas Boulevard and mixing ratios reached a maximum of 6 ppb. On 28 June,
468 m/z 69 and nonanal detected at m/z 143 ($C_9H_{18}OH^+$) are highly correlated ($r^2 > 0.93$), suggesting
469 that these ions share a common source. A similar correlation was observed between m/z 69 and
470 octanal ($r^2 = 0.90$).
471
472



473
474 **Figure 3.** Mobile laboratory data showing PTR-ToF-MS measurements of nonanal (m/z 143, $C_9H_{18}OH^+$, blue) and
475 m/z 69 ($C_9H_{18}H^+$, red) on the Las Vegas Strip during nighttime hours on (a) 28 June and (b) 30 July 2021. Mixing
476 ratios of m/z 69 are calculated assuming a sensitivity equivalent to isoprene. GC samples were only collected on 30
477 July, and the shaded regions in (b) show periods of sample collection (beige) and sample analysis (grey). The red
478 marker in (b) indicates the time of the GC-PTR-ToF-MS sample shown in Fig. 2.
479

480
481 Long-chain aldehydes are not routinely reported in urban datasets and the isoprene interference
482 due to aldehyde fragmentation is underappreciated in ambient PTR-ToF-MS datasets. Studies have
483 described how aldehydes produced on the surfaces of inlet tubing interfere with isoprene measured
484 by PTR-ToF-MS in remote forests (Vermeuel et al., 2022) and in the stratosphere (Ernle et al.,
485 2023), and aldehydes emitted from ocean surface waters also interfere with isoprene measurements
486 in laboratory studies and ambient measurements near coastal regions (Kilgour et al., 2021). Long-
487 chain aldehydes are likely ubiquitous in cities, and cooking activities are likely a major source of
488 octanal and nonanal resulting in an isoprene interference (Wernis et al., 2022; Peng et al., 2022).
489

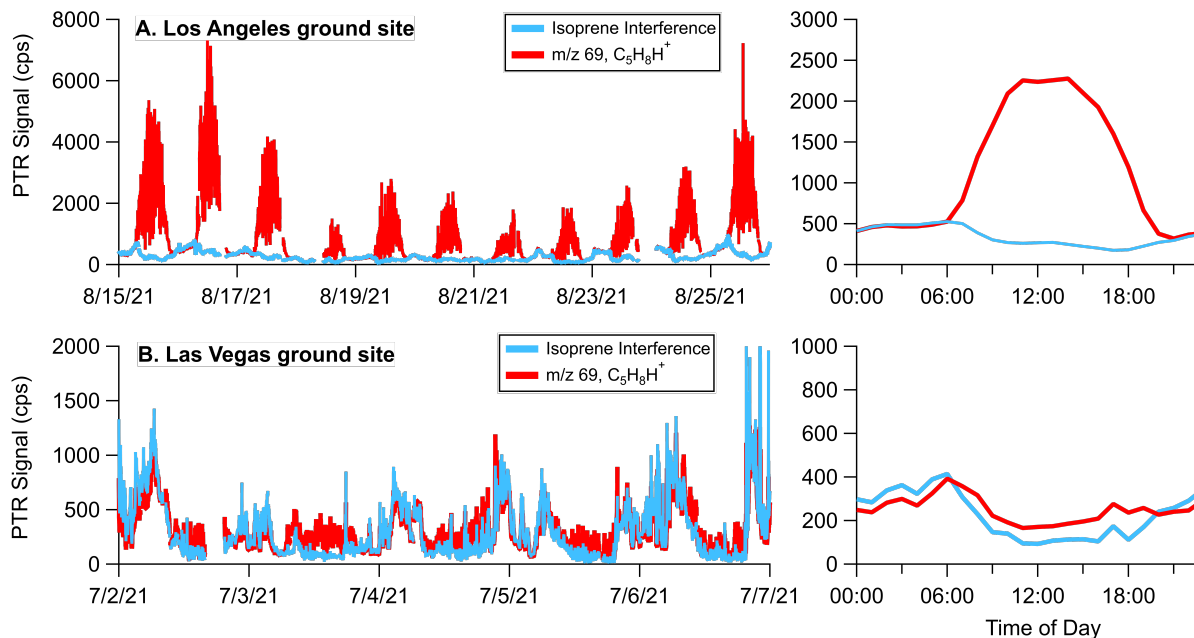
490 The interference from aldehydes is likely common across PTR designs, even though differences
491 could exist due to operating conditions (e.g., the E/N ratio). Figure S1 compares the fragmentation
492 patterns of pentanal, octanal, and nonanal observed in the NOAA PTR-ToF-MS (E/N ~ 140 Td),
493 which utilizes the Vocus ion source, to those reported by Buhr et al. (2002) (E/N ~120–130 Td),
494 which employ a traditional drift tube and quadrupole. In both reactor designs, C₅-aldehydes lose
495 neutral water to produce C₅H₈H⁺ (m/z 69) directly, while larger aldehydes such as octanal and
496 nonanal lose water to produce C₈H₁₅⁺ (m/z 111, exact mass: 111.117) and C₉H₁₇⁺ (m/z 125, exact
497 mass: 125.123), then further fragment to produce the C₅H₈H⁺ ion (Buhr et al., 2002; Pagonis et al.,
498 2019). These water-loss products are unique to aldehydes since ketone isomers do not undergo
499 significant fragmentation (Fig. S3).

500
501 We note that even though the fragmentation was similar between two instruments with different
502 reactor designs, fragmentation may result from the operation of other instrument components. For
503 example, the intensity of aldehyde fragmentation was found to vary strongly with voltage gradients
504 within the BSQ of the Berkeley Vocus-PTR-ToF-MS (Fig. S2). These results show that PTR-ToF-
505 MS systems employing quadrupole ion guides may exhibit fragmentation outside of the drift tube
506 region; consequently, care may be needed when tuning instruments to minimize unwanted
507 secondary reactions.

508 509 **3.1.3. Corrections to m/z 69 measured by NOAA PTR-ToF-MS during ground sampling in** 510 **Los Angeles and Las Vegas**

511
512 GC-PTR-ToF-MS and mobile laboratory measurements described in Section 3.1.2 indicate that
513 aldehydes significantly contribute to the signal at m/z 69 in urban areas. Chromatograms show that
514 the dehydration products from nonanal (m/z 125) and octanal (m/z 111) are useful markers that
515 distinguish aldehydes from ketone isomers. Coincidentally, the dehydration products from nonanal
516 and octanal are identical to the fragments produced from substituted cyclohexanes, which interfere
517 with isoprene in hydrocarbon-rich environments (see Gueneron et al., 2015; Warneke et al., 2014;
518 Pfannerstill et al., 2023b). Here, it is proposed that the signals at m/z 111 and m/z 125 can be used
519 as proxies to calculate the contribution from aldehyde and cycloalkane fragmentation on the signal
520 at m/z 69 in urban areas.

521
522 Figure 4 shows how the sum of m/z 111 and m/z 125 (termed the “isoprene interference”) varies
523 relative to the signal at m/z 69 measured by the NOAA PTR-ToF-MS at the ground sites in Los
524 Angeles and Las Vegas. In Los Angeles, high daytime emissions of isoprene dominate and
525 comprise most of the signal of m/z 69 from 6:00–19:00 LT. The high variability in the signal at
526 m/z 69 is caused by very localized emissions from trees upwind of the measurement site. In Las
527 Vegas, isoprene emissions are much lower and the diel pattern of m/z 69 closely follows the
528 behavior of the isoprene interference with only small additional signal during the daytime.
529



530
 531 **Figure 4.** Time series and diurnal pattern of the signal at m/z 69 ($C_5H_8H^+$) and the isoprene interference (m/z 111 +
 532 m/z 125) measured at the (a) Los Angeles and (b) Las Vegas ground sites by the NOAA PTR-ToF-MS. The time
 533 series data are shown for select periods to illustrate correlations between the isoprene interference and m/z 69. The
 534 diel patterns on the right are campaign averages.
 535

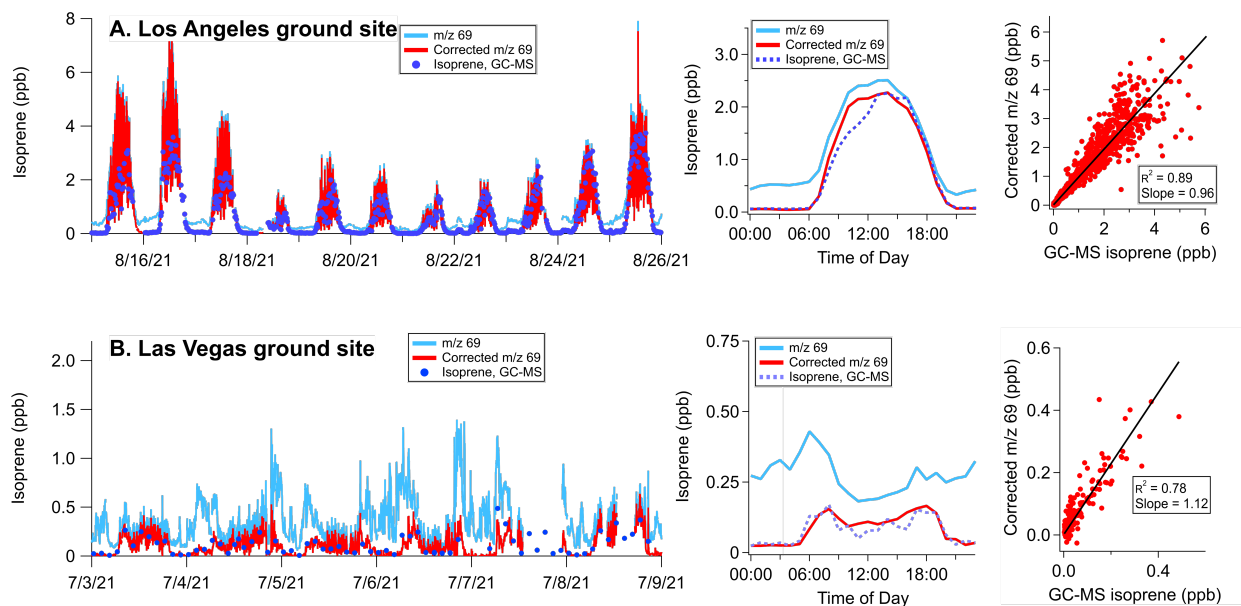
536
 537 Biogenic isoprene is predominantly emitted during daytime hours (e.g., Guenther et al., 2012),
 538 while the isoprene interference in both cities is more prevalent at night. These differences in diurnal
 539 patterns can be leveraged to subtract interferences from aldehydes and cycloalkanes from PTR-
 540 ToF-MS measurements of m/z 69. Here, the signals at m/z 69, m/z 111, and m/z 125 are analyzed
 541 between 00:00-04:00 LT when daytime isoprene from biogenic sources is expected to be low. The
 542 instrument response to aldehyde and cycloalkane fragmentation is calculated by determining the
 543 ratio of m/z 69 to the sum of m/z 111 + m/z 125. This ratio is then applied to the full dataset
 544 following Eq. 1.
 545

$$546 \quad m/z\ 69_{\text{Corrected}} = S_{69} - S_{111+125} \cdot f_{69/(111+125)} \quad (1)$$

547
 548 S_{69} is the signal measured at m/z 69, $S_{111+125}$ is the signal of the isoprene interference (sum of m/z
 549 111 + m/z 125), and $f_{69/(111+125)}$ is the interference ratio determined at night. The nighttime
 550 interference ratio in Las Vegas (3.1) and Los Angeles (3.6) is shown in Fig. S4. This interference
 551 ratio is determined using an orthogonal distance regression to account for errors in the signals at
 552 m/z 69, 111, and 125. The differences between the cities may reflect variations in the distribution
 553 of aldehydes and cycloalkanes.
 554

555 Figure 5 shows how measurements of m/z 69 change as a result of this correction and compares
 556 the corrected/calculated isoprene mixing ratios to the GC-MS measurements co-located with the
 557 PTR-ToF-MS. In Los Angeles, the correction largely impacts m/z 69 signals at night. The diurnal
 558 pattern shows that average mixing ratios approach zero in the evenings, though increases in
 559 nighttime isoprene mixing ratios are observed during some periods (e.g., 22–24 August, Fig. S5).
 560 Corrections to m/z 69 during the daytime lead to a ~ 10% decrease in reported mixing ratios. This

561 shows that even when isoprene emissions are high, VOC fragmentation can have a significant
 562 impact on the signal at m/z 69.
 563



564
 565 **Figure 5.** Uncorrected and corrected m/z 69 as time series, diel averages, and correlation plots for (a) the Los Angeles
 566 and (b) Las Vegas ground sites. GC-MS measurements are shown for comparison against the corrected m/z 69
 567 isoprene mixing ratios. A detailed comparison of nighttime isoprene corrections in Los Angeles is shown in Fig. S5.
 568 The best fits are determined using ODR
 569

570 The corrected m/z 69 measurements are well correlated with GC-MS isoprene measurements (r^2
 571 = 0.89) and agree to within 4%. At high isoprene mixing ratios, the measurements exhibit a greater
 572 degree of scatter. This variability likely results from the differences in sampling timescales (1 s for
 573 PTR-ToF-MS, ~ 240 s for GC-MS and 120s for WAS samples) along with the high variability of
 574 isoprene emissions from trees at the measurement site. When averaged to a diel profile, the daytime
 575 mixing ratios also agree to within 4%. Both instruments show that average isoprene decreases to
 576 low mixing ratios at night (< 0.05 ppb). The GC-MS observed a number of periods of enhanced
 577 nighttime isoprene, likely from non-biogenic sources. Remarkably, after accounting for the
 578 isoprene interference, the corrected m/z 69 mixing ratios from the PTR-ToF-MS captures the
 579 variability in nighttime isoprene observed by GC-MS in Los Angeles (Fig. S5). On average, the
 580 isoprene interference represents ~90% of the nighttime signal of m/z 69.
 581

582 The isoprene correction is most impactful on the Las Vegas measurements where isoprene
 583 emissions are low and aldehydes + cycloalkane fragments constitute a larger fraction of the signal
 584 at m/z 69. Without correction, the variability in m/z 69 across all daytime hours is driven by the
 585 isoprene interference (Fig. 4). After the interference contributions are subtracted, corrected
 586 isoprene mixing ratios approach zero at night and decrease by nearly 50% to 0.1–0.15 ppb during
 587 the day (Fig. 5b). The resulting diel pattern changes substantially and exhibits a daytime peak that
 588 is consistent with the expected pattern for isoprene. GC-MS measurements show that isoprene
 589 mixing ratios were typically < 0.2 ppb and the corrected m/z 69 diel pattern generally matches the
 590 average diel pattern of isoprene reported by GC-MS. Though the number of canister samples in

591 Las Vegas were limited (total 275, sampled every 2–4 h), a comparison between the corrected m/z
592 69 and GC-MS isoprene shows that the measurements agree to within 15%.

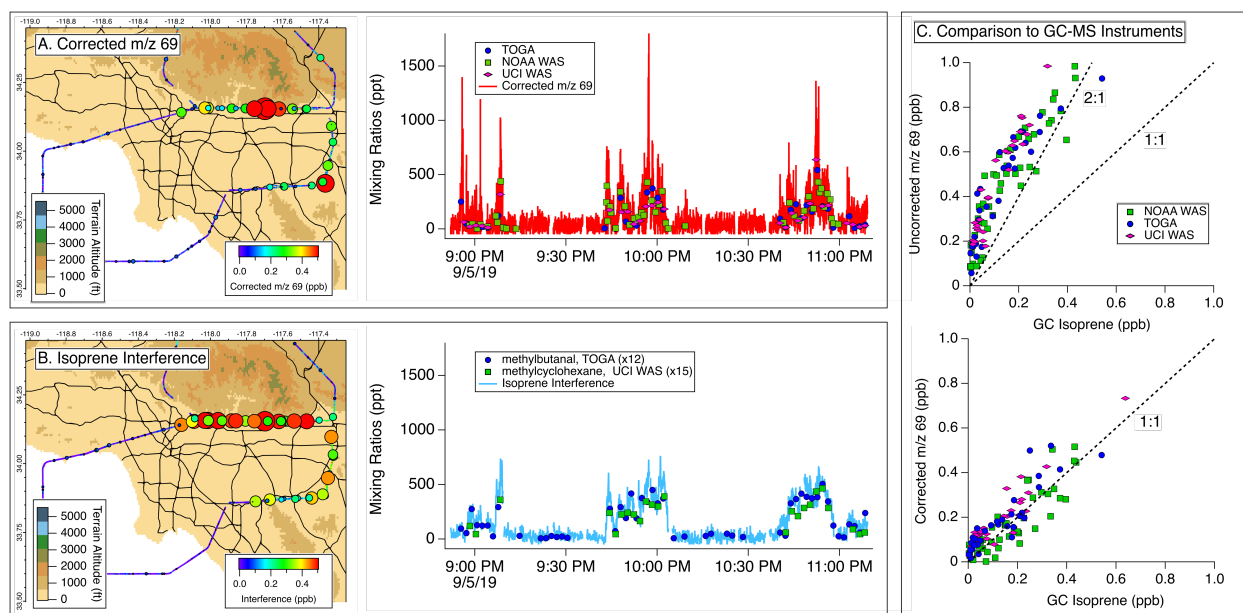
593
594 **3.1.4. Corrections to m/z 69 measured by NOAA and Oslo PTR-ToF-MS during airborne**
595 **sampling over Los Angeles**

596
597 The isoprene interferences observed during SUNVEx and RECAP-CA show that PTR-ToF-MS
598 measurements of m/z 69 are significantly impacted by aldehydes and cycloalkanes. To assess the
599 impact of isoprene interferences at higher altitudes, we analyze the FIREX-AQ and RECAP-CA
600 measurements of flights in the Los Angeles Basin and determine corrected m/z 69 signals
601 following Eq. (1). One challenge to this approach is that the DC-8 and Twin Otter aircraft did not
602 sample the Los Angeles Basin at night, and therefore the interference ratio ($f_{69/(111+125)}$) is not easily
603 determined in the absence of isoprene. To overcome this limitation for FIREX-AQ, we vary the
604 interference ratio until the corrected m/z 69 signals reported by the NOAA PTR-ToF-MS matches
605 with the isoprene mixing ratios reported by GC instrumentation on the DC-8. The resulting ratio
606 determined by iteration (4.4) is ~ 20% higher than the ratio determined at ground level during
607 SUNVEx (3.6), which likely reflects differences between the operating conditions and drift tube
608 designs used on the NOAA PTR-ToF-MS during FIREX-AQ and SUNVEx (traditional vs.
609 Vocus).

610
611 Figure 6 illustrates the spatial and temporal variability in (a) the corrected m/z 69 mixing ratios
612 and (b) the calculated interference. Transits to the north show that the interference is highest along
613 the San Gabriel Mountains where anthropogenic pollution typically builds in the Los Angeles
614 Basin (Angevine et al., 2013) and reached mixing ratios as high as 500 ppt. The interference
615 correlates well with both methylcyclohexane measured by the UCI WAS and methylpropanal
616 measured by TOGA-TOF, which are proxies for the species known to fragment to produce the
617 isoprene interference (i.e., cycloalkanes and aldehydes). Corrected m/z 69 mixing ratios only
618 exhibit significant enhancements in regions where the DC-8 sampled air close to vegetation. Short
619 bursts of isoprene were observed above the San Gabriel Mountains, but mixing ratios were
620 typically lower than 500 ppt. Over the entire flight, the isoprene interference constituted > 50% of
621 the signal observed at m/z 69.

622
623 Figure 6c compares the PTR-ToF-MS measurements to GC-based samples for uncorrected m/z 69
624 (top) and corrected m/z 69 mixing ratios (bottom). These comparisons show that the isoprene
625 interference resulted in an overestimation of PTR-ToF-MS measurements of isoprene by at least a
626 factor of 2. At times, the NOAA PTR-ToF-MS measured mixing ratios of m/z 69 that were 5 times
627 larger than the isoprene mixing ratios reported by GC-based methods. The Oslo PTR-ToF-MS also
628 sampled onboard the DC8 during FIREX-AQ and presented an opportunity to compare to the
629 fragmentation observed by the NOAA PTR-TOF-MS. Following a similar correction procedure as
630 described above, Fig. S6 shows that the Oslo PTR-ToF-MS measured the same degree of
631 interferences as the NOAA PTR-ToF-MS (i.e., fragmentation biased isoprene measurements high
632 by at least a factor of 2). The consistency between both instruments demonstrates that isoprene
633 interferences are common across PTR-ToF-MS designs (i.e., TOFWERK vs. Ionicon).

634



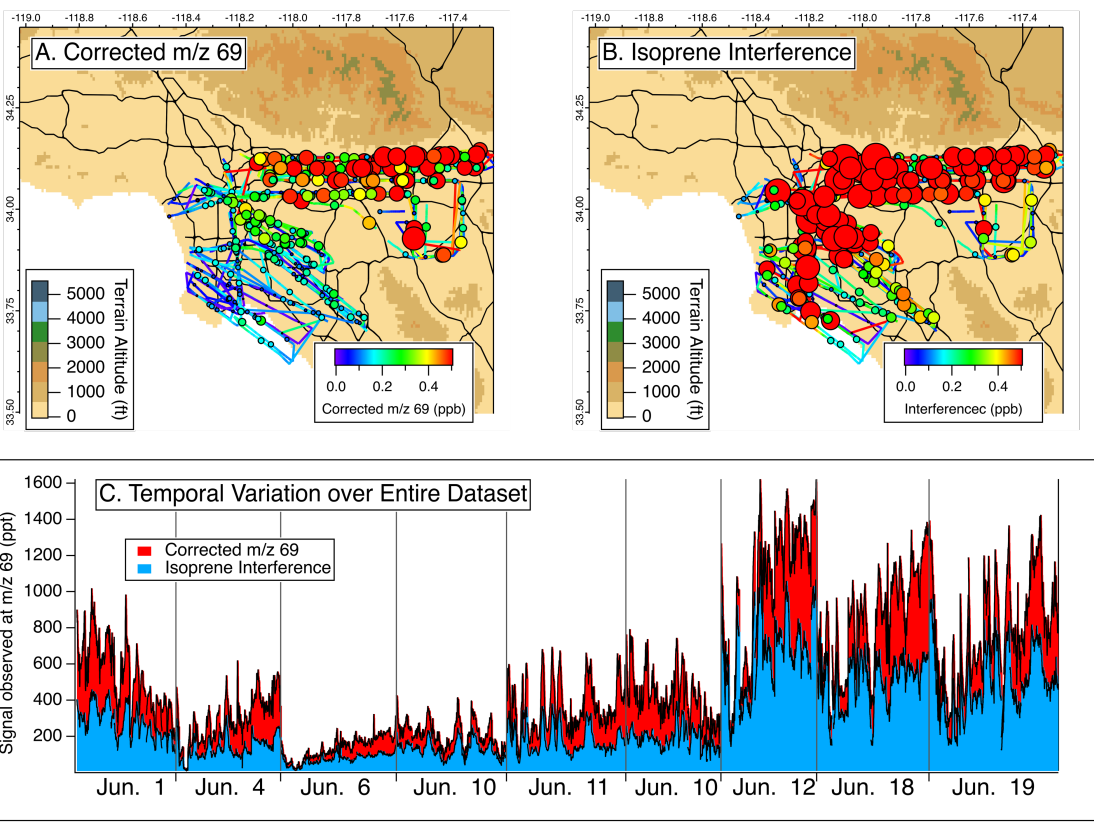
635
 636 **Figure 6.** Impact of isoprene interference correction on m/z 69 measurements from the NOAA PTR-ToF-MS during
 637 FIREX-AQ. (a) Map of corrected m/z 69 distribution (left) and time series with corresponding measurements of
 638 isoprene from GC-MS samples (right). (b) Map of isoprene interference (left) and time series with GC-MS
 639 measurements of methylcyclohexane and methylpropanal, which are proxies for cycloalkanes and aldehydes known
 640 to contribute to the signal at m/z 69. (c) Comparisons of PTR-ToF-MS measurements of m/z 69 and GC-based isoprene
 641 mixing ratios for uncorrected m/z 69 (top) and corrected m/z 69 (bottom) using Eq. (1) with an interference ratio =
 642 10.
 643

644 3.1.5. Corrections to m/z 69 measured by Berkeley PTR-ToF-MS during airborne sampling 645 over Los Angeles 646

647 The Berkeley Vocus PTR-ToF-MS also observed interferences to m/z 69 during the RECAP-CA
 648 flights. Unlike FIREX-AQ, GC-MS measurements were not available onboard the Twin Otter to
 649 compare against PTR-ToF-MS measurements. To evaluate the interference contributions to m/z
 650 69 here, we determine the interference ratio from nonanal calibrations and compare it with data
 651 collected from the Central Valley and Los Angeles Basin. In these regions, the signal at m/z 69
 652 and the sum of m/z 111 + 125 are well-correlated with a slope that closely matches the measured
 653 fragmentation pattern for nonanal (Fig. S7). The interference ratio observed in the Central Valley
 654 where oil and natural gas emissions are significant is similar to the ratio observed in Los Angeles
 655 where aldehydes are more important. In the Central Valley, periods of high biogenic influence are
 656 clearly separated from periods of high interference from anthropogenic emissions. Building on
 657 these responses, we use the calibrated data for nonanal to derive an m/z 69 correction in Los
 658 Angeles. This method is limited in accounting for molecules that have fragmentation ratios
 659 differing from nonanal, but since the interference ratio observed from oil and gas regions and from
 660 the Los Angeles Basin is similar to the nonanal fragmentation ratio, we expect the uncertainty to
 661 be relatively small despite there being no GC comparison.
 662

663 Figure 7 shows the impact of the isoprene interference on the Berkeley PTR-ToF-MS data. The
 664 Twin Otter flew nine flights and the total signal of m/z 69 varied between 200–1200 ppt. Similar
 665 to the observations by the NOAA PTR-ToF-MS during FIREX-AQ, the isoprene interference
 666 during RECAP-CA was at least 50% of the signal observed at m/z 69 (Fig. 7c). The Twin Otter

667 sampled a larger swath of area than the DC-8, and Fig. 7 shows that the interference is persistent
 668 across the Los Angeles Basin (Fig. 7b) at mixing ratios as high as 600 ppt. Similar to the DC-8
 669 flight, corrected m/z 69 mixing ratios are highest along the San Gabriel Mountains. The Twin Otter
 670 is capable of sampling at lower altitudes than the DC-8, and therefore larger mixing ratios of
 671 isoprene were observed.
 672
 673

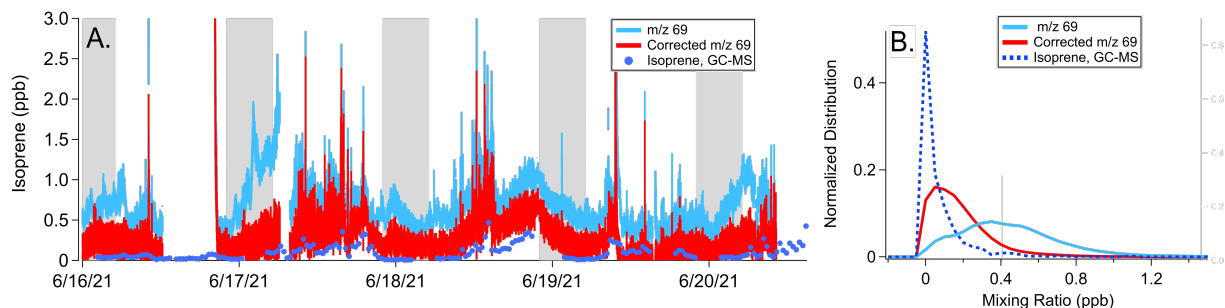


674
 675 **Figure 7.** Impact of isoprene interference correction on isoprene measurements during RECAP-CA as (a) the corrected
 676 isoprene distribution, (b) the isoprene interference, and (c) a pseudo time series of the total m/z 69 signal colored by
 677 the contributions of corrected m/z 69 and isoprene interference for all flights.
 678

679 The contribution of the isoprene interference observed from the aircraft with the Berkeley PTR-
 680 ToF-MS differs from the observations by the NOAA PTR-ToF-MS at Caltech during RECAP-
 681 CA. On the ground, the isoprene interference observed by the NOAA PTR-ToF-MS was ~10% of
 682 the signal at m/z 69 during daytime hours (Fig. 5a), while at altitude the Berkeley PTR-ToF-MS
 683 observed an interference > 50%. This difference can be explained by (1) the abundance of isoprene
 684 emitters close to the ground site, (2) the differences in reactivities between isoprene, aldehydes,
 685 and cycloalkanes, and (3) the different instrument setting of the Berkeley PTR-ToF-MS (Fig. S2).
 686 Isoprene is highly reactive towards atmospheric oxidants such as the OH radical ($k_{OH} \sim 1 \times 10^{-10}$
 687 $\text{cm}^3 \text{ molecule}^{-1} \text{ s}^{-1}$), whereas saturated aldehydes and cycloalkanes are expected to be 5–10 times
 688 less reactive (Burkholder et al., 2019). This difference in reactivity may alter the distribution of
 689 VOCs that contribute to m/z 69 and result in higher interferences aloft. The DC-8 and Twin Otter
 690 aircraft did not specifically target altitude profiling while sampling in the Los Angeles Basin, but
 691 future work may help to characterize the impact of the isoprene interference at other altitudes.
 692

693 **3.1.6. Corrections to m/z 69 measured by Aerodyne PTR-ToF-MS during ground sampling**
694 **in Detroit, MI**
695

696 The SUNVEx/RECAP-CA/FIREX-AQ data reflect the behavior of the NOAA, Oslo, and Berkeley
697 instruments during summertime measurements in Los Angeles. Isoprene interferences likely
698 impact ground and airborne measurements in other cities and at other times of year. Figure 8 shows
699 the impact of interferences to the signal at m/z 69 reported by the Aerodyne PTR-ToF-MS
700 measurements during MOOSE. This campaign targeted emissions in Detroit, MI, where the
701 Aerodyne Mobile Laboratory conducted a mix of mobile and stationary sampling in select
702 locations around the metropolitan area (Fig. 1). Figure 8a shows a subset of PTR-ToF-MS
703 measurements of m/z 69 and corrected m/z 69, along with isoprene measurements by the Aerodyne
704 GC-MS. Corrected m/z 69 is calculated by determining the interference ratio at night (2.54),
705 similar to the approach used to calculate interferences during SUNVEx/RECAP-CA. Figure 8b
706 shows normalized histograms for each measurement over the entire deployment.
707



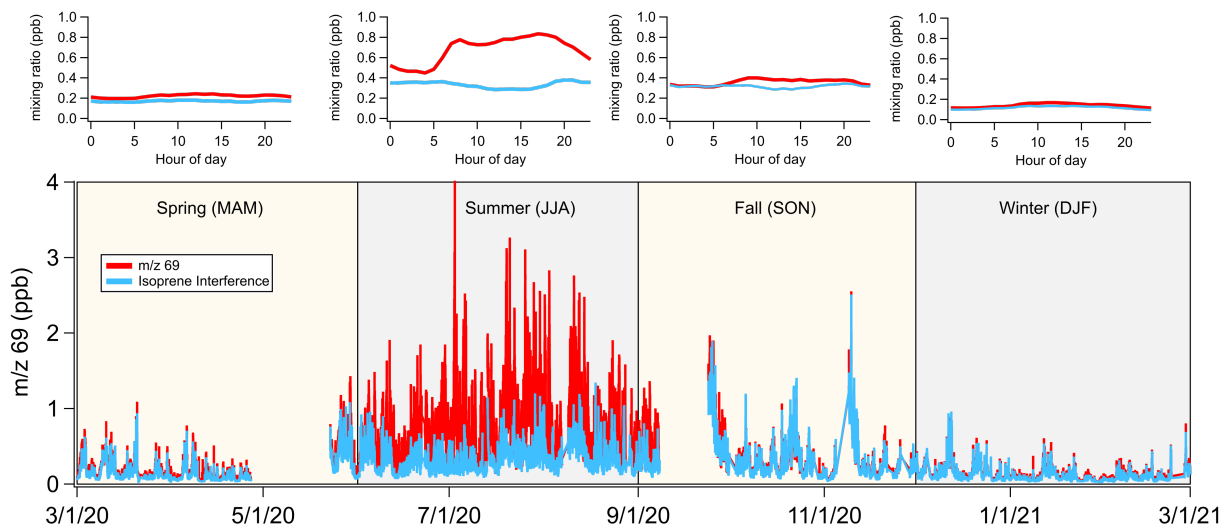
708 **Figure 8.** Impact of isoprene interference correction on the PTR-ToF-MS data collected from the Aerodyne Mobile
709 Laboratory during the MOOSE campaign as a (a) time series of GC-MS measurements, uncorrected and corrected
710 m/69 isoprene mixing ratios. The shaded regions show nighttime measurements (22:00–05:00 LT). (b) Histograms
711 showing the distribution of m/z 69 measured by the Aerodyne PTR-ToF-MS, corrected m/z 69 isoprene mixing ratios,
712 and isoprene mixing ratios measured by the GC-MS.
713

714
715 Without correction, m/z 69 reported by PTR-ToF-MS exhibits a broad distribution with a peak
716 mixing ratio of ~ 0.4 ppb (Fig. 8b). After applying the corrections described by Eq. (1), m/z 69
717 signals decrease by nearly a factor of 2 and show better agreement with isoprene reported by GC-
718 MS. Corrected m/z 69 mixing ratios are still a factor of 2 higher than the isoprene mixing ratios
719 reported by the GC-MS. One possibility is that other VOCs in the Detroit region may also
720 contribute to the signal at m/z 69. GC pre-separation measurements directly using PTR-ToF-MS
721 were not conducted during MOOSE; consequently, it is difficult to determine what other species
722 might contribute to m/z 69 in this region. Broad deployment of GC-PTR-ToF-MS measurements
723 in urban areas may help to better quantify the contributions of fragmenting species to PTR-ToF-
724 MS measurements of m/z 69.
725

726 **3.1.7. Seasonal changes to the m/z 69 interferences observed by the Stony Brook PTR-ToF-**
727 **MS in New York City**
728

729 Figure 9 shows the impact of the isoprene interference on data reported by the Stony Brook PTR-
730 ToF-MS during a year-long sampling effort to characterize emissions in New York City during
731 the COVID-19 lockdown. Shown here are mixing ratios of m/z 69 along with the estimated
732 contribution to m/z 69 from the isoprene interference. We calculate the isoprene interference for

733 each season, and present the diurnal patterns in the top row. The interference ratio ($f_{69/(111+125)}$, Eq.
 734 (1)) is similar in spring, summer, and winter (2.2–2.5), but lower during fall (1.9).
 735



736
 737 **Figure 9.** (bottom) Time series of m/z 69 and isoprene interference measured by the Stony Brook PTR-ToF-MS at
 738 the urban ASRC ground site in New York City. (top) Diel patterns of m/z 69 and isoprene interference
 739 mixing ratios for each season.

740
 741 The signal at m/z 69 is variable across seasons and the highest mixing ratios are observed during
 742 summer. The isoprene interference is a major contributor to m/z 69 in fall, winter, and spring (77-
 743 88% of total signal) and strongly influences the day-to-day variability. During summertime
 744 isoprene emissions from urban foliage increases the variability in m/z 69 and results in higher
 745 mixing ratios of m/z 69 during the day. The isoprene interference increases the background mixing
 746 ratios of m/z 69 and dominates the total signal at night.

747
 748 The ASRC site is located in a heavily urbanized region and the PTR-ToF-MS sampled air at the
 749 top of the building where mixing ratios of isoprene are likely lower. The persistent, high
 750 contribution from the isoprene interference to m/z 69 during all seasons likely reflects the high
 751 emissions of aldehydes and cycloalkanes from anthropogenic sources in this region. Figure S8
 752 contrasts the measurements at ASRC with those reported from the Flax Pond site. Flax Pond is
 753 located in a less-densely populated region of Long Island where biogenic sources of isoprene are
 754 more abundant. There, interferences are a much smaller fraction of the signal at m/z 69 (< 10%)
 755 and the variability is largely driven by isoprene during the summer months. Mixing ratios at Flax
 756 Pond are lower during the winter, but comparable to those observed at ASRC during the same
 757 season (~ 100–150 ppt). Furthermore, the variability is predominantly driven by the isoprene
 758 interference. Figures 9 and S8 demonstrate that interferences will vary spatially between heavily
 759 urban and biogenic-dominated regions. In addition, outside of the summer months, isoprene is
 760 unlikely to be a major contributor to m/z 69 in both regions.

761
 762 **3.1.8. Implications of the m/z 69 correction on estimates of biogenic isoprene**
 763

764 The contribution of the isoprene interference to m/z 69 in New York City is comparable to the
765 ground level measurements in Las Vegas, Los Angeles, and Detroit (0.25–0.5 ppb), which
766 demonstrates that isoprene measurements by PTR-MS are significantly impacted across most, if
767 not all, urban regions. The interferences to m/z 69 are highest at night and in the wintertime;
768 consequently, identifying anthropogenic or nighttime sources of isoprene by PTR-MS will be
769 difficult if not confirmed unambiguously by GC-PTR-ToF-MS or separately by GC-MS.

770
771 The measurements in Los Angeles, Las Vegas, and New York City show that interferences may
772 bias daytime measurements of m/z 69 (and thus, estimates of isoprene) by as much as a factor of
773 2 depending on the location or sampling altitude. Isoprene is a major contributor to OH reactivity
774 and ozone production in these regions (McDonald et al., 2018b) and measurements from high-
775 time-resolution instruments are often used to validate biogenic emissions inventories used in air
776 quality models (e.g., Coggon et al., 2021; Pfannerstill et al., 2023a; McDonald et al., 2018b).
777 Corrections to PTR-ToF-MS data are important when comparing m/z 69 mixing ratios to biogenic
778 emissions inventories in urban areas so that isoprene emissions are not overestimated in air quality
779 models. PTR-ToF-MS measurements may also be used to determine isoprene fluxes. Due to the
780 differences in spatial variability between interferences and biogenic isoprene, estimates of isoprene
781 fluxes may be less sensitive to the impact of aldehyde or cycloalkene fragmentation (Pfannerstill
782 et al., 2023a; Pfannerstill et al., 2023b).

783 784 **3.2. Oxygenated VOCs**

785 786 **3.2.1. Characterizing interferences to oxygenated VOCs using GC-PTR-ToF-MS**

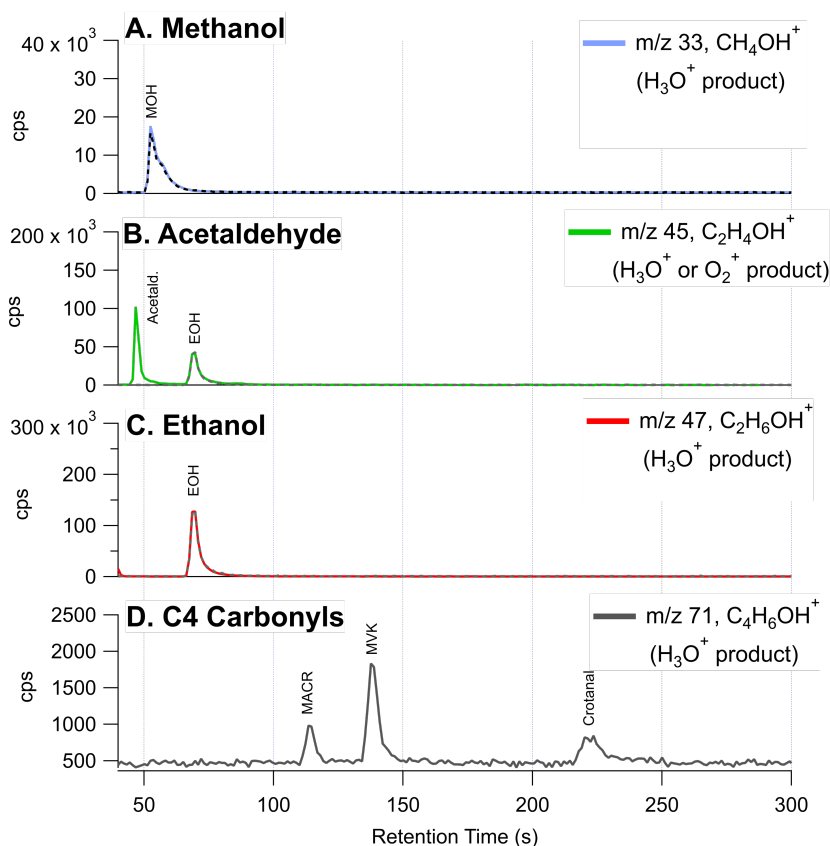
787
788 Small oxygenated VOCs are an important contributor to the reactivity and ozone produced in urban
789 areas. Alcohols, ketones, and small aldehydes (< C₄) may be emitted to the atmosphere from
790 mobile sources, VCPs, cooking activities, and other sources (Klein et al., 2016; McDonald et al.,
791 2018a), but are also formed as secondary products of atmospheric chemistry. Some studies have
792 reported that certain alcohols, such as ethanol, may ionize to product products that overlap with
793 proton-transfer products of other important oxygenates, such as acetaldehyde (Buhr et al., 2002;
794 Pagonis et al., 2019). Previous intercomparisons have shown that acetaldehyde is one example of
795 oxygenated VOCs where there may be large disagreements between PTR-ToF-MS and GC-MS
796 (Yuan et al., 2016).

797
798 Figure 10 shows the GC-PTR-ToF-MS chromatogram collected on the Las Vegas Strip for proton-
799 transfer products typically assigned to oxygenated VOCs. Here, we present small oxygenates
800 typically reported in ambient data sets that are subject to fragmentation or interferences, including
801 methanol, acetaldehyde, ethanol, and C₄-carbonyls, which represent the sum of methacrolein
802 (MACR), methyl vinyl ketone (MVK), and crotonaldehyde.

803
804 First, GC-PTR-ToF-MS data show that no other species elute through the GC column to yield a
805 significant interference to methanol and ethanol. The signal at m/z 59 (C₃H₆OH⁺) is also observed
806 to result entirely from acetone + propanal (not shown). This is consistent with previous studies
807 that show good agreement between GC-MS and PTR-ToF-MS (e.g., Warneke et al., 2003).

808

809 Crotonaldehyde is a major fraction of the C₄-carbonyls observed on the Las Vegas Strip. Typically,
 810 MVK and MACR are treated as the dominant isomers to the C₄-carbonyl product (m/z 71,
 811 C₄H₆OH⁺), since these are secondary products from isoprene oxidation and are expected to be
 812 present at high mixing ratios (Yuan et al., 2017). Crotonaldehyde is observed to be a major
 813 contributor to m/z 71 in biomass burning emissions (Koss et al., 2018), but its presence on the Las
 814 Vegas Strip likely points to other important aldehyde sources, such as cooking. The higher fraction
 815 of crotonaldehyde reflects that isoprene mixing ratios are lower in Las Vegas than other cities (Fig.
 816 5) and that cooking is an important source of VOCs along the Las Vegas Strip (Fig. 2). Xu et al.
 817 (2022) showed that measurements of C₄-carbonyls by the NOAA PTR-ToF-MS, ammonium-
 818 adduct chemical ionization mass spectrometer (NH₄-CIMS), and NOAA GC-MS agreed in the
 819 daytime during RECAP-CA when MVK and MACR were high, but disagreed at night when
 820 isoprene products were low and crotonaldehyde mixing ratios were likely elevated. Additional
 821 interferences at m/z 71 could result from decomposition of ISOPOOH on inlet surfaces (Rivera-
 822 Rios et al., 2014).
 823



824
 825 **Figure 10.** GC-PTR-ToF-MS chromatograms from the Las Vegas Strip showing the contributions of isomers and
 826 fragments to ions typically assigned to small oxygenates. The labels highlight the traditionally assigned isomers for
 827 (a) methanol, (a) acetaldehyde, (c) ethanol, and (d) C₄-carbonyls including methacrolein (MACR), methyl vinyl ketone
 828 (MVK), and crotonaldehyde.
 829

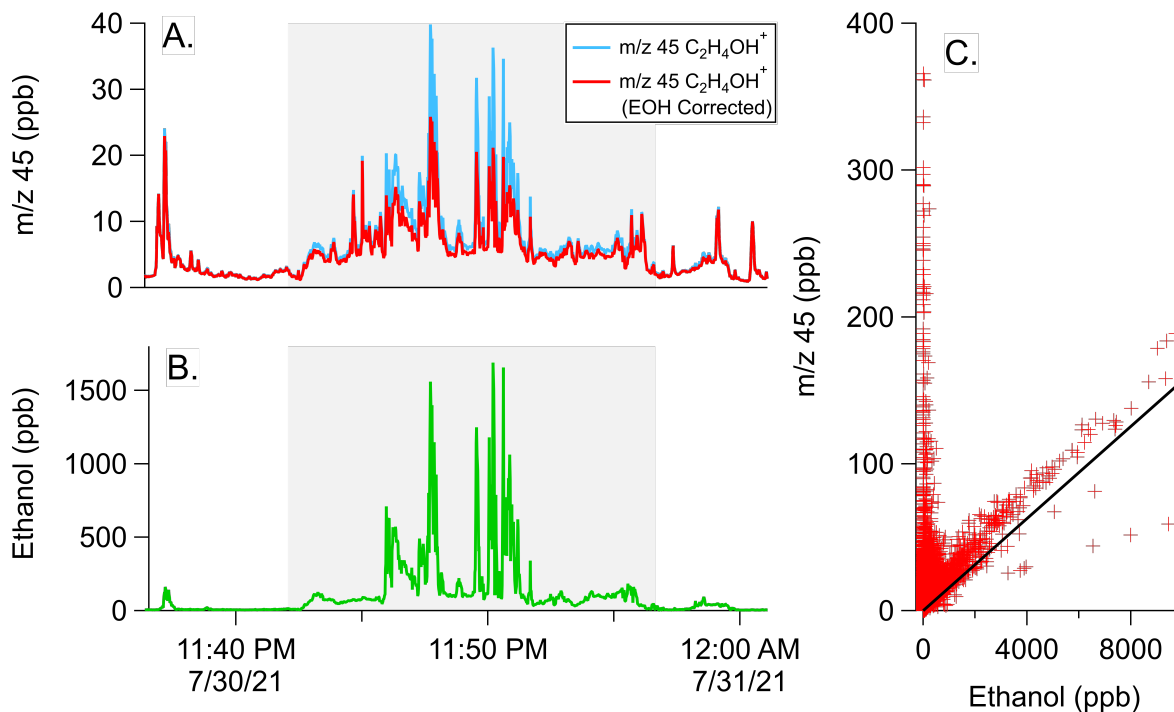
830 3.2.2. Interferences to m/z 45 from ethanol reactions with O₂⁺

831
 832 The most significant interference for the small oxygenated VOCs observed by GC-PTR-ToF-MS
 833 is associated with the ionization of ethanol to produce signal at the mass typically assigned to

834 acetaldehyde (m/z 45, $C_2H_5O^+$). Ethanol has been shown by Inomata and Tanimoto (2009) to
835 produce fragments at m/z 19 (H_3O^+), m/z 31 (CH_3O^+), and m/z 29 ($C_2H_5^+$). Buhr et al. (2002)
836 identified m/z 45 as product and found that it correlated to the ethanol proton transfer product (m/z
837 47, $C_2H_6OH^+$) with a ratio of 0.22. The likely pathway for the formation of m/z 45 is by ethanol
838 reactions with O_2^+ , which has been identified by Spänzel and Smith (1997) as the dominant O_2^+
839 product using selective ion flow tube (SIFT) mass spectrometry. The NOAA Vocus PTR-ToF-MS
840 observes a ratio that is higher than that determined by Buhr et al. (2002) (~ 0.38), although the
841 distribution of total fragmentation (i.e., the sum of all ethanol fragments relative to m/z 47) appears
842 similar (Fig. S1).

843
844 Figure 11 shows the temporal behavior of m/z 45 and m/z 47 (ethanol) during the nighttime drive
845 on 30 July. Figure 11a shows the mixing ratio of m/z 45 assuming the sensitivity of acetaldehyde
846 and Fig. 11b shows the mixing ratio of ethanol. Figure 11c shows a scatter plot of the signal at m/z
847 45 vs. that of m/z 47 for the entire mobile laboratory dataset. First, ethanol and m/z 45 are
848 correlated when ethanol mixing ratios are high (Fig. 11a, b). Ethanol on the Las Vegas Strip
849 reached mixing ratios of 1.5 ppm and corresponding increases in m/z 45 were observed that point
850 towards a contribution from ethanol. Figure 11c shows that a subset of the m/z 45 signal measured
851 throughout the Las Vegas dataset exhibit a ratio to ethanol that agrees with the fragmentation ratio
852 observed from GC-PTR-ToF-MS measurements. These observations point towards a broader
853 impact of ethanol on m/z 45 throughout the Las Vegas region.

854



855
856 **Figure 11.** Demonstration of impacts of ethanol on mobile drive data in downtown Las Vegas during the evening
857 drive on 30 July. (a) Time series of the signal at m/z 45 ($C_2H_4OH^+$) with and without the subtraction of the ethanol
858 interference. (b) Time series of ethanol (m/z 47, $C_2H_6OH^+$). The shaded regions show when the mobile laboratory was
859 sampling along the Las Vegas strip. (c) Correlation plot of mobile drive data for the entire Las Vegas dataset. The
860 solid line shows the fragmentation ratio of m/z 45 to m/z 47 for ethanol, as derived from the GC-PTR-ToF-MS data
861 (Fig. 10).

862

863 3.2.3. Corrections to m/z 45 measured by NOAA PTR-ToF-MS during ground sampling in 864 Las Vegas

865
866 The extent to which ethanol contributed to the signal at m/z 45 can be determined by correction
867 techniques. Figure 11a shows the m/z 45 signal with the contribution from ethanol subtracted
868 following:

$$869 \quad m/z\ 45\ \text{Corrected} = S_{45} - S_{47} \cdot f_{45/47} \quad (2)$$

870
871
872 S_{45} is the signal from m/z 45, S_{47} is the signal of ethanol, and $f_{45/47}$ is the ratio determined by GC-
873 PTR-ToF-MS. Generally, the ethanol-corrected data on m/z 45 show that ethanol contributed
874 ~40% to the signal on the Las Vegas Strip. Outside of this region, ethanol ionization has a modest
875 impact on m/z 45. Over the average mobile laboratory dataset, ethanol may have contributed as
876 much as 5% to the total signal at m/z 45. Similar contributions are estimated for the ground site
877 data collected during ground sampling in Los Angeles. Consequently, ethanol reactions with O_2^+
878 may only be an important contributor to m/z 45 in highly-concentrated ethanol plumes, which may
879 be encountered during mobile sampling or upon aircraft encounters with point sources. This ratio
880 may also be affected by humidity, which changes the distribution of O_2^+/H_3O^+ in drift tubes
881 operated at low water mixing ratio. The TOFWERK and Ionicon instruments have fundamental
882 design differences that impact O_2^+ production and relatively humidity responses. Ionicon
883 instruments have a separate region where excess water and air are pumped away from the ion
884 source. In these instruments, O_2^+ production is low since diffusion of air into the discharge region
885 is mitigated, but changes to ambient relative humidity may result in alterations to the primary ion
886 distribution. In contrast, ions and excess water are passed through the Vocus in Tofwerk
887 instruments. The water content in the drift tube is high resulting in negligible humidity responses
888 (Krechmer et al., 2018), but air in the drift tube may diffuse to the ion source to produce O_2^+ .

889
890 The GC-PTR-ToF-MS provides some insights into the interferences of oxygenates, but there are
891 limits to the extent to which oxygenates elute through a DB-624 or other GC columns with similar
892 polarity. Interferences towards oxygenated masses may be an important focus for future work, as
893 recent studies have pointed towards the increasing fraction of oxygenated VOCs observed in urban
894 air (Karl et al., 2018; Xu et al., 2022; Khare et al., 2022) and instrumentation capable of measuring
895 unfragmented oxygenates are becoming more common (e.g., Khare et al., 2022; Xu et al., 2022;
896 Riva et al., 2019). Intercomparisons with GC-MS measurements employing polar columns, or with
897 mass spectrometers employing softer ionization chemistry (e.g., iodide or NH_4^+ adduct mass
898 spectrometers) may help to better characterize the response and selectivity of PTR-ToF-MS to
899 oxygenates.

900 901 3.3. Aromatic VOCs

902 903 3.3.1. Known interferences to aromatic masses

904
905 PTR-ToF-MS is well suited to measure ambient mixing ratios of C_6 – C_9 aromatics; however, it is
906 known that alkyl aromatics (e.g., ethylbenzene and ethyltoluene isomers) and aromatic
907 monoterpenes and monoterpenoids (e.g., cymene and fenchone, Kari et al., 2018; Tani, 2013)
908 fragment and contribute to the signals typically attributed to benzene (m/z 79, $C_6H_6H^+$) and toluene

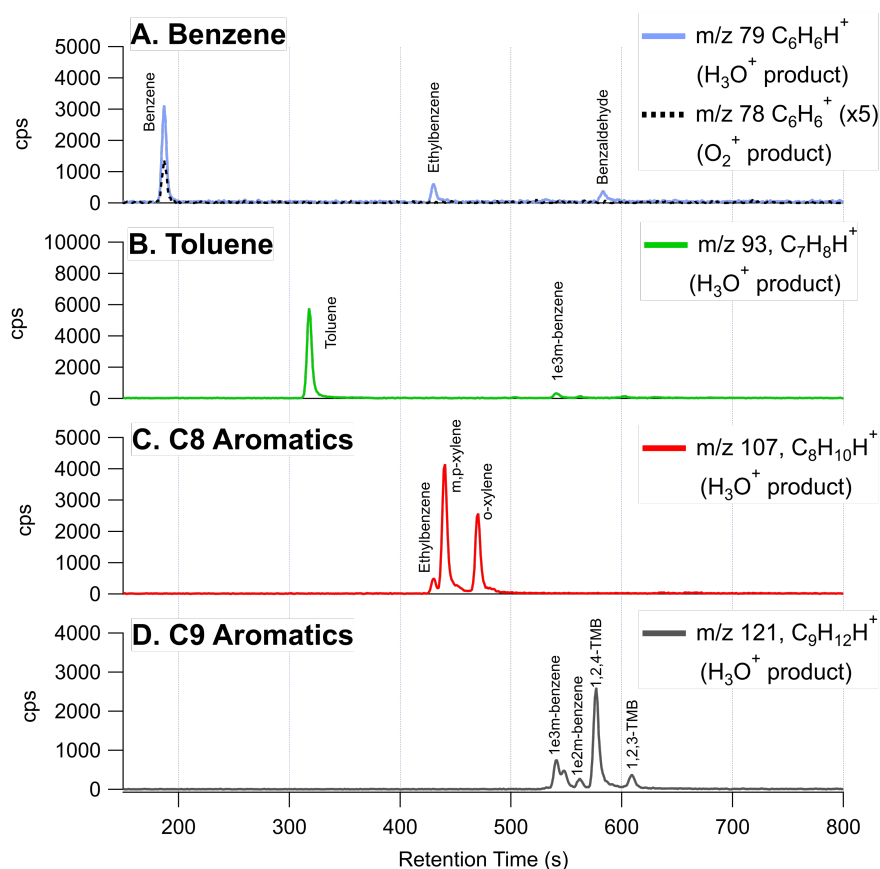
909 (m/z 93, $C_7H_8H^+$) (Pagonis et al., 2019; Yuan et al., 2017). The abundance and distribution of
 910 aromatics depends on the relative mix of VOC emissions from petrochemical sources, including
 911 fossil fuels, solvents emitted from VCPs (e.g. paints and architectural coatings), and asphalt paving
 912 (Gkatzelis et al., 2021a; Gkatzelis et al., 2021b; Khare et al., 2020; Stockwell et al., 2021). Higher
 913 aromatics, such as xylenes and ethylbenzene, are prevalent in both fossil fuel and VCP emissions,
 914 whereas benzene is restricted in consumer products and is therefore almost entirely associated with
 915 fossil fuels (McDonald et al., 2018a). Consequently, PTR-ToF-MS measurements in urban regions
 916 with significant solvent emissions may exhibit a greater degree of interference on benzene and
 917 toluene than regions with greater fossil fuel usage.

918

919 3.3.2. Characterizing interferences to m/z 79 using GC-PTR-ToF-MS

920

921 Figure 12 shows GC-PTR-ToF-MS measurements of key aromatic compounds measured in
 922 downtown Las Vegas where both fossil fuels and VCP emissions were prevalent. Each panel is
 923 labeled by the typical compound assignment and shows chromatograms of the corresponding
 924 proton-transfer product. In general, chromatograms show that C_9 - and C_8 -aromatics are the
 925 expected key contributors to the signals at m/z 121 ($C_9H_{12}H^+$) and m/z 107 ($C_8H_{10}H^+$),
 926 respectively. This is consistent with previously observed PTR-ToF-MS behavior (Yuan et al.,
 927 2017), and shows that urban measurements at these masses continue to be reliably assigned to
 928 simple alkyl aromatics.



929

930 **Figure 12.** GC-PTR-ToF-MS chromatogram from downtown Las Vegas showing the contributions of isomers and
 931 fragments to ions typically assigned to C_6 – C_9 aromatics. The labels highlight the traditionally assigned isomers for (a)

932 benzene, (b) toluene, (c) C₈-aromatics including *o,m,p*-xylene + ethylbenzene, and (d) C₉-aromatics including
933 ethyltoluene isomers + trimethylbenzene isomers.

934
935 In contrast, the masses typically assigned to benzene (m/z 79, C₆H₆H⁺) and toluene (m/z 93,
936 C₇H₈H⁺) show greater contributions from the fragmentation of alkyl aromatics. At m/z 93, most
937 of the signal is attributed to toluene and a small fraction (< 5%) results from the fragmentation of
938 1-ethyl-3-methylbenzene. At m/z 79, ~ 80% of the signal results from the proton-transfer product
939 of benzene and the remainder from the fragmentation of ethylbenzene and benzaldehyde. Previous
940 work has shown contributions of ethylbenzene to m/z 79 in urban air (Inomata et al., 2010),
941 whereas contributions from benzaldehyde are not well studied. Benzaldehyde may result from
942 VCPs, cooking, motor vehicle emissions, biomass burning, or secondary production (Gkatzelis et
943 al., 2021a; Koss et al., 2018; McDonald et al., 2018a).

944 945 **3.3.3. Corrections to m/z 79 measured by NOAA PTR-ToF-MS during ground sampling in** 946 **Los Angeles and Las Vegas**

947
948 The interferences at m/z 79 are significant and present a challenge for reliably quantifying benzene
949 in Las Vegas and other urban regions. To quantify this interference, Fig. 13 highlights benzene
950 measurements from the Las Vegas and Los Angeles ground sites. Figure 13a, b show corrected
951 and uncorrected benzene at m/z 79 can be attributed to benzene calculated from two methods:

$$952$$
$$953 \quad m/z\ 79_{\text{Corrected}} = S_{\text{C}_6\text{H}_6\text{H}^+} - S_{\text{C}_7\text{H}_6\text{OH}^+} \cdot f_{79/\text{Benzald}} - S_{\text{C}_8\text{H}_{10}\text{H}^+} \cdot f_{79/\text{Ethylbenzene}} \quad (\text{Method 1})$$
$$954$$

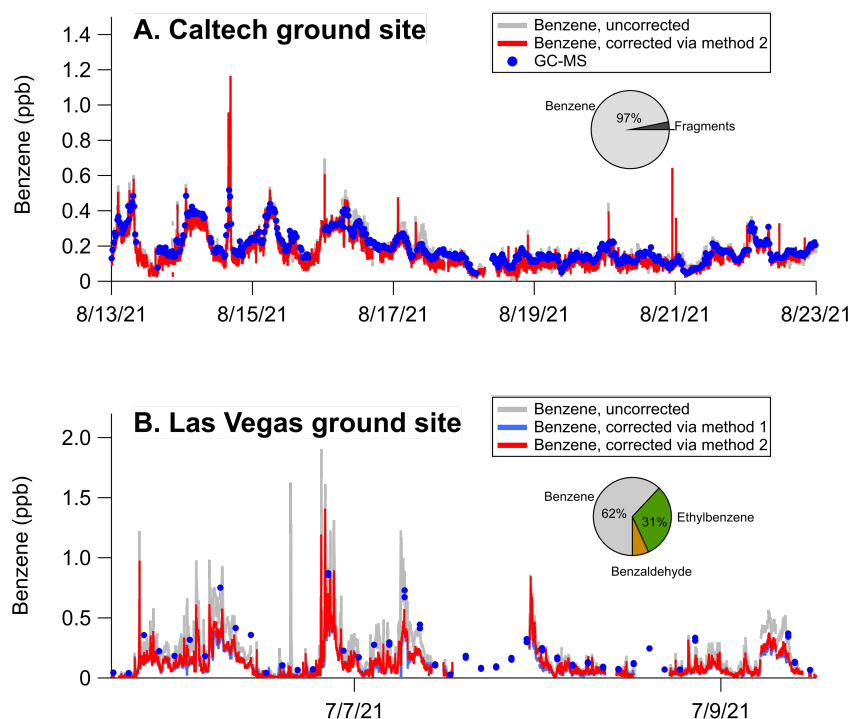
$$955$$
$$956 \quad m/z\ 79_{\text{Corrected}} = S_{\text{C}_6\text{H}_6^+} \quad (\text{Method 2})$$
$$957$$

958
959 Where S_{C₆H₆H⁺} is the signal of C₆H₆H⁺, S_{C₇H₆OH⁺} is the signal attributable to benzaldehyde, S_{C₈H₁₀H⁺}
960 is the signal attributable to ethylbenzene, and S_{C₆H₆⁺} is the signal attributed to the benzene charge-
961 transfer product at m/z 78. f_{79/Benzald} and f_{79/Ethylbenzene} are the fragmentation patterns of
962 benzaldehyde (f_{79/Benzald} = C₆H₆H⁺/C₇H₆OH⁺) and ethylbenzene (f_{79/Ethylbenzene} = C₆H₆H⁺/C₈H₁₀H⁺)
963 as determined by GC-PTR-ToF-MS chromatograms. Method 1 corrects for benzene by subtracting
964 the contributions of benzaldehyde and ethylbenzene to the signal at C₆H₆H⁺. GC-PTR-ToF-MS
965 measurements show that benzaldehyde is the primary contributor to S_{C₇H₆OH⁺}, whereas
966 ethylbenzene is one of four isomers that contributes to S_{C₈H₁₀H⁺}. We use the GC-PTR-ToF-MS
967 measurements at the Las Vegas ground site and find that ethylbenzene contributes ~12.5% of the
968 total C₈-aromatic signal. Method 2 simply estimates benzene mixing ratios based on calibrations
969 applied to the charge-transfer product at m/z 78 (C₆H₆⁺). This mass has no discernible interference
970 from other VOCs in the GC-PTR-ToF-MS data (Fig. 12) and is detected with sufficient sensitivity
971 to reliably quantify benzene (~180 cps ppb⁻¹). We note that Method 1 requires regular
972 quantification of C₈-aromatic distributions by GC in order to account for ethylbenzene
973 fragmentation, whereas Method 2 relies only on measurements of the O₂⁺ charge-transfer product.
974 We note that Method 2 may present limitations if other species are present that fragment to produce
975 the O₂⁺ product or if a PTR-ToF-MS response to the O₂⁺ depends on humidity or ion source design.
976 Deployment of GC-PTR-ToF-MS in other cities may help to determine whether the charge-
977 transfer product is unambiguously linked to benzene.

978

979 On average, the interferences from ethylbenzene and benzaldehyde constitute ~ 38% of the signal
 980 at m/z 79 detected in Las Vegas, and ~ 3% of signal detected in Los Angeles (pie charts, Fig 13).
 981 We speciate the interference in Las Vegas using GC-PTR-ToF-MS and find that the majority of
 982 the interference is associated with fragmentation of ethylbenzene (31% of total signal) with a small
 983 contribution from benzaldehyde (7% of total signal). Ethylbenzene was likely emitted from a local
 984 source due to a cabinet-making shop upwind of the ground site. The two methods for correcting
 985 benzene agree well for Las Vegas data, which confirms that ethylbenzene and benzaldehyde are
 986 the primary contributors to the benzene interferences. We note that we only use Method 2 for data
 987 collected in Los Angeles since GC-PTR-ToF-MS measurements were unavailable during this
 988 period of the deployment.
 989

990



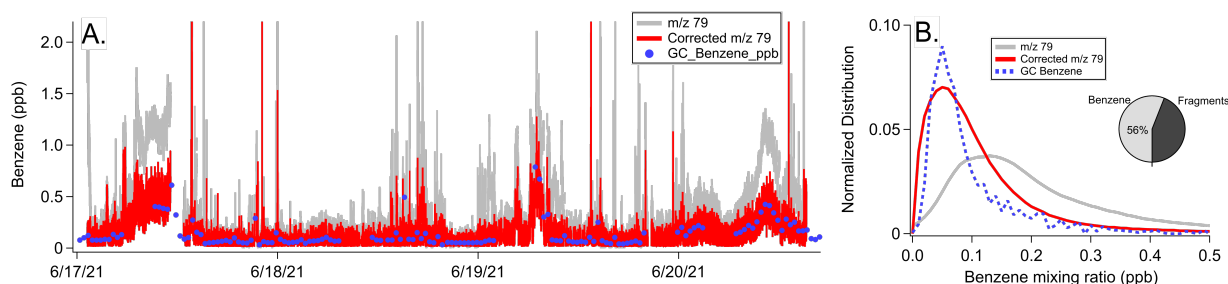
991 **Figure 13.** Impact of fragmentation on the signal at m/z 79 ($C_6H_6H^+$) and corresponding benzene mixing ratios
 992 measured in (a) Los Angeles and (b) Las Vegas. The corrections using the two methods are shown compared to
 993 uncorrected data. The pie charts show the average contribution of benzene, ethylbenzene, and benzaldehyde to the
 994 signal at m/z 79 ($C_6H_6H^+$).
 995

996

997 **3.3.4. Corrections to m/z 79 measured by Aerodyne PTR-ToF-MS during ground sampling**
 998 **in Detroit**
 999

1000 The significant interferences to m/z 79 observed in Las Vegas are also observed in PTR-ToF-MS
 1001 data collected downwind of Detroit during the MOOSE campaign. Figure 14 shows four days of
 1002 mobile laboratory sampling with the Aerodyne PTR-ToF-MS and GC-MS instrumentation.
 1003 Similar to Fig. 13, corrected via Method 2 and uncorrected m/z 79 measurements are shown (Fig.
 1004 14a). Figure 14b shows the histograms of PTR-ToF-MS measurements alongside those from the
 1005 GC-MS during the entire campaign. The pie chart shows the average fraction of m/z 79 attributed

1006 to benzene vs. the fraction associated with fragments. Benzaldehyde and ethylbenzene
1007 contributions are not separated since GC-PTR-ToF-MS measurements were unavailable.
1008
1009



1010
1011 **Figure 14.** (a) Time series of GC-MS samples of benzene and PTR-ToF-MS mixing ratios of m/z 79 ($C_6H_6H^+$) and
1012 corrected m/z 79 reported during sampling by the Aerodyne Mobile Laboratory downwind of Detroit, MI. (b)
1013 Histograms showing the distribution of m/z 79 measured by the Aerodyne PTR-ToF-MS, corrected m/z 79 mixing
1014 ratios calculated using Method 2, and benzene mixing ratios measured by the GC-MS. The pie chart highlights the
1015 fraction of the m/z 79 associated with benzene vs. the fraction associated with fragments.
1016

1017 Similar to Las Vegas, fragmentation of higher aromatic species plays an important role in
1018 determining the benzene signal in m/z 79. The distribution of uncorrected m/z 79 shows a peak
1019 around 0.12 ppb and a broad tail biased towards higher mixing ratios. The GC-MS measures a
1020 distribution of benzene with a maximum at 0.05 ppb, and a much lower frequency of higher mixing
1021 ratios. When the PTR-ToF-MS data are calibrated using the benzene charge-transfer product
1022 (Method 2), corrected m/z 79 mixing ratios show a better agreement with GC-MS measurements.
1023 The distribution of corrected m/z 79 is wider than that reported by GC-MS, which may reflect the
1024 faster sampling of the PTR-ToF-MS and more frequent observations of concentrated aromatic
1025 plumes (Fig. 14a). Over the entire sampling period, the average distribution of m/z 79 shows that
1026 benzene accounts for $\sim 56\%$ of the total signal. This is consistent with the observations in Las
1027 Vegas (interference $\sim 62\%$ of the signal), indicating that m/z 79 in both datasets were influenced
1028 by solvent emissions to a significant extent.
1029

1030 4. Conclusions

1031
1032 Urban VOCs significantly contribute to the degradation of air quality, and PTR-ToF-MS provides
1033 important constraints on the emissions and chemical transformation of many gas-phase organics.
1034 Advances in PTR-ToF-MS sensitivity and detection provide opportunities to identify, characterize,
1035 and revisit measurement interferences to commonly reported VOCs (Yuan et al., 2017). Here, we
1036 find that long-chain aldehydes, along with previously identified cycloalkanes, are important
1037 contributors to the signal of m/z 69 typically associated with isoprene in many urban areas. The
1038 fragmentation of these molecules can be larger than the signal associated with the proton-transfer
1039 product from isoprene, depending on the mixture of anthropogenic and biogenic VOCs, time of
1040 day, and season. We find that interferences at ground level in Los Angeles (large isoprene
1041 emissions, large anthropogenic emissions) are highest at night and constitute $\sim 10\%$ of the signal
1042 observed during the day. Interferences are a higher fraction of m/z 69 at altitude ($> 50\%$) and are
1043 observed to be widespread throughout the Los Angeles Basin. In Las Vegas (low isoprene
1044 emissions, large anthropogenic emissions), interferences dominate the signal at m/z 69 throughout
1045 the day and night. These interferences are observed in other cities (e.g., Detroit and New York

1046 City), depend on season, and are common among drift tube designs operated at similar E/N.
1047 Corrections to PTR-ToF-MS measurements at m/z 69 are necessary in order to capture the air
1048 quality impacts of isoprene in urban areas.

1049
1050 Other PTR-ToF-MS masses also exhibit interferences, including those typically assigned to
1051 oxygenates and aromatic VOCs. Fragmentation from ethanol impacts measurements of
1052 acetaldehyde on m/z 45, though this interference is only significant in regions with large ethanol
1053 emissions. PTR-ToF-MS measurements of benzene using m/z 79 exhibit significant interferences
1054 from the fragmentation of ethylbenzene and benzaldehyde. In Las Vegas and Detroit,
1055 fragmentation impacts m/z 79 mixing ratios by as much as 40%. The growing contribution of
1056 interferences to aromatics and oxygenates may reflect the changing mix of urban VOC emissions
1057 from one dominated by mobile sources to one dominated by solvents (Gkatzelis et al., 2021b;
1058 McDonald et al., 2018a). In the case of benzene, other ions such as the charge-transfer product
1059 (m/z 78, C₆H₆⁺) can be used to quantify benzene without significant influence from fragmentation
1060 from higher carbon VOCs. As instrument sensitivity improves, there may be other ions that can be
1061 used to improve the quantification of additional VOCs. These ions may differ across instrument
1062 designs depending on the ion source design and response to ambient relative humidity.

1063
1064 Corrections to these interferences are feasible, though it is unlikely that a universal correction
1065 factor is sufficient to resolve instrument discrepancies across datasets. Instrument responses, as
1066 well as changes to the VOC mixture in different regions, require that detailed characterization be
1067 performed on a dataset-by-dataset basis. GC-MS measurements provide an opportunity to compare
1068 against PTR-ToF-MS measurements for a wide-variety of key VOCs, including isoprene, small
1069 oxygenates, and aromatics. Likewise, information about fragmentation and instrument-specific
1070 responses to reactive hydrocarbons can be determined using GC-PTR-ToF-MS. For species such
1071 as oxygenates, intercomparisons against other mass spectrometers using softer ionization (e.g.,
1072 iodide or ammonium-adduct CIMS) or use of GC pre-separation using polar columns may yield
1073 valuable information about instrument artifacts.

1074 1075 **Data Availability**

1076
1077 Data for SUNVEx and RE-CAP are available at the NOAA CSL data repository
1078 (<https://csl.noaa.gov/projects/sunvex/>). Data for FIREX-AQ, MOOSE, and LISTOS are available
1079 at the NASA data repository (<https://www-air.larc.nasa.gov/missions.htm>).

1080 1081 **Author Contribution**

1082
1083 MMC, CES, XL, JBG, AL, CW, EYP, CA, EFK, and AHG conducted measurements during
1084 SUNVEx and RE-CAP. MMC, GIG, CW, JBG, AL, AW, FP, DB, RH, and ECA conducted
1085 measurements during FIREX-AQ. MSC, BML, FM, and MC conducted measurements during
1086 MOOSE. JM, CC, and JEM conducted measurements during LISTOS. MMC and CW wrote the
1087 paper with contributions from all authors.

1088 1089 **Competing Interests**

1090

1091 EAC is a co-editor of Atmospheric Measurement Techniques. The peer-review process was guided
1092 by an independent editor and the authors also have no other competing interests to declare.

1093

1094 **Acknowledgements**

1095

1096 MMC, CES, XL, JBG, and CW acknowledge funding from Clark County, NV (contract number
1097 20-022001) and the California Air Resources Board (contract number 20RD002). All authors
1098 thank Paul Wennberg, John Seinfeld, and Ben Schulze for their coordination of the Caltech ground
1099 site. JM, CC, and JM acknowledge funding from the Northeast States for Coordinated Air Use
1100 Management (NESCAUM) through a contract with the New York State Energy Research and
1101 Development Authority (NYSERDA) (agreement number 101132). AHG, EYP, EFK, and CA
1102 acknowledge funding from the California Air Resources Board (contract number 20RD003,
1103 20AQP012), NOAA Climate Program Office's Atmospheric Chemistry, Carbon Cycle, and
1104 Climate program (contract number NA22OAR4310540 [UCB]/ NA22OAR4310541 [AD]). the
1105 Office of Naval Research Defense University Research Instrumentation Program (grant number
1106 N00014-19-1-2108), and EPA-STAR (grant number 84001001). EYP was supported by a Feodor
1107 Lynen Fellowship of the Alexander von Humboldt Foundation.

1108

1109 **References**

1110

1111 Angevine, W. M., Brioude, J., McKeen, S., Holloway, J. S., Lerner, B. M., Goldstein, A. H., Guha,
1112 A., Andrews, A., Nowak, J. B., Evan, S., Fischer, M. L., Gilman, J. B., and Bon, D.: Pollutant
1113 transport among California regions, *Journal of Geophysical Research: Atmospheres*, 118, 6750-
1114 6763, <https://doi.org/10.1002/jgrd.50490>, 2013.

1115 Annual Monitoring Network Plan, Clark County Department of Environment and Sustainability,
1116 1-77, 2022.

1117 Apel, E. C., Hornbrook, R. S., Hills, A. J., Blake, N. J., Barth, M. C., Weinheimer, A., Cantrell, C.,
1118 Rutledge, S. A., Basarab, B., Crawford, J., Diskin, G., Homeyer, C. R., Campos, T., Flocke, F., Fried,
1119 A., Blake, D. R., Brune, W., Pollack, I., Peischl, J., Ryerson, T., Wennberg, P. O., Crouse, J. D.,
1120 Wisthaler, A., Mikoviny, T., Huey, G., Heikes, B., O'Sullivan, D., and Riemer, D. D.: Upper
1121 tropospheric ozone production from lightning NO_x-impacted convection: Smoke ingestion case
1122 study from the DC3 campaign, *Journal of Geophysical Research: Atmospheres*, 120, 2505-2523,
1123 <https://doi.org/10.1002/2014JD022121>, 2015.

1124 Arata, C., Misztal, P. K., Tian, Y., Lunderberg, D. M., Kristensen, K., Novoselac, A., Vance, M. E.,
1125 Farmer, D. K., Nazaroff, W. W., and Goldstein, A. H.: Volatile organic compound emissions
1126 during HOMEChem, *Indoor Air*, 31, 2099-2117, <https://doi.org/10.1111/ina.12906>, 2021.

1127 Arnold, S. T., Viggiano, A. A., and Morris, R. A.: Rate Constants and Product Branching Fractions
1128 for the Reactions of H₃O⁺ and NO⁺ with C₂-C₁₂ Alkanes, *The Journal of Physical Chemistry A*,
1129 102, 8881-8887, 10.1021/jp9815457, 1998.

- 1130 Breitenlechner, M., Fischer, L., Hainer, M., Heinritzi, M., Curtius, J., and Hansel, A.: PTR3: An
1131 Instrument for Studying the Lifecycle of Reactive Organic Carbon in the Atmosphere, *Analytical*
1132 *Chemistry*, 89, 5824-5831, [10.1021/acs.analchem.6b05110](https://doi.org/10.1021/acs.analchem.6b05110), 2017.
- 1133 Buhr, K., van Ruth, S., and Delahunty, C.: Analysis of volatile flavour compounds by Proton
1134 Transfer Reaction-Mass Spectrometry: fragmentation patterns and discrimination between
1135 isobaric and isomeric compounds, *International Journal of Mass Spectrometry*, 221, 1-7,
1136 [https://doi.org/10.1016/S1387-3806\(02\)00896-5](https://doi.org/10.1016/S1387-3806(02)00896-5), 2002.
- 1137 Burkholder, J. B., Sander, S. P., Abbatt, J., Barker, J. R., Cappa, C., Crouse, J. D., Dibble, T. S.,
1138 Huie, R. E., Kolb, C. E., Kurylo, M. J., Orkin, V. L., Percival, C. J., Wilmouth, D. M., and Wind, P. H.:
1139 Chemical Kinetics and Photochemical Data for Use in Atmospheric Studies, Evaluation No. 19,
1140 Jet Propulsion Laboratory, Pasadena, CA, 2019.
- 1141 Calfapietra, C., Fares, S., Manes, F., Morani, A., Sgrigna, G., and Loreto, F.: Role of Biogenic
1142 Volatile Organic Compounds (BVOC) emitted by urban trees on ozone concentration in cities: A
1143 review, *Environmental Pollution*, 183, 71-80, <https://doi.org/10.1016/j.envpol.2013.03.012>,
1144 2013.
- 1145 Cao, C., Gentner, D. R., Commane, R., Toledo-Crow, R., Schiferl, L. D., and Mak, J. E.: Policy-
1146 Related Gains in Urban Air Quality May Be Offset by Increased Emissions in a Warming Climate,
1147 *Environmental Science & Technology*, [10.1021/acs.est.2c05904](https://doi.org/10.1021/acs.est.2c05904), 2023.
- 1148 Choi, J., Henze, D. K., Cao, H., Nowlan, C. R., González Abad, G., Kwon, H.-A., Lee, H.-M., Oak, Y.
1149 J., Park, R. J., Bates, K. H., Maasakkers, J. D., Wisthaler, A., and Weinheimer, A. J.: An Inversion
1150 Framework for Optimizing Non-Methane VOC Emissions Using Remote Sensing and Airborne
1151 Observations in Northeast Asia During the KORUS-AQ Field Campaign, *Journal of Geophysical*
1152 *Research: Atmospheres*, 127, e2021JD035844, <https://doi.org/10.1029/2021JD035844>, 2022.
- 1153 Claflin, M. S., Pagonis, D., Finewax, Z., Handschy, A. V., Day, D. A., Brown, W. L., Jayne, J. T.,
1154 Worsnop, D. R., Jimenez, J. L., Ziemann, P. J., de Gouw, J., and Lerner, B. M.: An in situ gas
1155 chromatograph with automatic detector switching between PTR- and EI-TOF-MS: isomer-
1156 resolved measurements of indoor air, *Atmos. Meas. Tech.*, 14, 133-152, [10.5194/amt-14-133-](https://doi.org/10.5194/amt-14-133-2021)
1157 [2021](https://doi.org/10.5194/amt-14-133-2021), 2021.
- 1158 Coggon, M. M., McDonald, B. C., Vlasenko, A., Veres, P. R., Bernard, F., Koss, A. R., Yuan, B.,
1159 Gilman, J. B., Peischl, J., Aikin, K. C., DuRant, J., Warneke, C., Li, S.-M., and de Gouw, J. A.:
1160 Diurnal Variability and Emission Pattern of Decamethylcyclopentasiloxane (D5) from the
1161 Application of Personal Care Products in Two North American Cities, *Environmental Science &*
1162 *Technology*, 52, 5610-5618, [10.1021/acs.est.8b00506](https://doi.org/10.1021/acs.est.8b00506), 2018.
- 1163 Coggon, M. M., Gkatzelis, G. I., McDonald, B. C., Gilman, J. B., Schwantes, R. H., Abuhassan, N.,
1164 Aikin, K. C., Arend, M. F., Berkoff, T. A., Brown, S. S., Campos, T. L., Dickerson, R. R., Gronoff, G.,
1165 Hurley, J. F., Isaacman-VanWertz, G., Koss, A. R., Li, M., McKeen, S. A., Moshary, F., Peischl, J.,
1166 Pospisilova, V., Ren, X., Wilson, A., Wu, Y., Trainer, M., and Warneke, C.: Volatile chemical

1167 product emissions enhance ozone and modulate urban chemistry, *Proceedings of the National*
1168 *Academy of Sciences*, 118, e2026653118, doi:10.1073/pnas.2026653118, 2021.

1169 Colman, J. J., Swanson, A. L., Meinardi, S., Sive, B. C., Blake, D. R., and Rowland, F. S.:
1170 Description of the Analysis of a Wide Range of Volatile Organic Compounds in Whole Air
1171 Samples Collected during PEM-Tropics A and B, *Analytical Chemistry*, 73, 3723-3731,
1172 10.1021/ac010027g, 2001.

1173 Ernle, L., Ringsdorf, M. A., and Williams, J.: Influence of ozone and humidity on PTR-MS and GC-
1174 MS VOC measurements with and without a Na₂S₂O₃ ozone scrubber, *Atmos. Meas. Tech.*, 16,
1175 1179-1194, 10.5194/amt-16-1179-2023, 2023.

1176 Gkatzelis, G. I., Coggon, M. M., McDonald, B. C., Peischl, J., Aikin, K. C., Gilman, J. B., Trainer, M.,
1177 and Warneke, C.: Identifying Volatile Chemical Product Tracer Compounds in U.S. Cities,
1178 *Environmental Science & Technology*, 55, 188-199, 10.1021/acs.est.0c05467, 2021a.

1179 Gkatzelis, G. I., Coggon, M. M., McDonald, B. C., Peischl, J., Gilman, J. B., Aikin, K. C., Robinson,
1180 M. A., Canonaco, F., Prevot, A. S. H., Trainer, M., and Warneke, C.: Observations Confirm that
1181 Volatile Chemical Products Are a Major Source of Petrochemical Emissions in U.S. Cities,
1182 *Environmental Science & Technology*, 55, 4332-4343, 10.1021/acs.est.0c05471, 2021b.

1183 Gkatzelis, G. I., Coggon, M. M., Stockwell, C. E., Hornbrook, R. S., Allen, H., Apel, E. C., Bela, M.
1184 M., Blake, D. R., Bourgeois, I., Brown, S. S., Campuzano-Jost, P., St. Clair, J. M., Crawford, J. H.,
1185 Crouse, J., Day, D. A., DiGangi, J. P., Diskin, G. S., Fried, A., Gilman, J. B., Guo, H., Hair, J. W.,
1186 Halliday, H. S., Hanisco, T. F., Hannun, R. A., Hills, A., Huey, L. G., Jimenez, J. L., Katich, J. M.,
1187 Lamplugh, A., Lee, Y. R., Liao, J., Neuman, J. A., Nowak, J. B., Pagonis, D., Peischl, J., Perring, A.
1188 E., Piel, F., Rickly, P. S., Robinson, M. A., Rollins, A. W., Ryerson, T. B., Schueneman, M. K.,
1189 Schwantes, R. H., Schwarz, J. P., Sekimoto, K., Selimovic, V., Shingler, T., Tanner, D. J., Tomsche,
1190 L., Vasquez, K. T., Veres, P., Washenfelder, R. A., Weibring, P., Wennberg, P. O., Wisthaler, A.,
1191 Wolfe, G. M., Womack, C. C., Xu, L., Yokelson, R., and Warneke, C.: Parameterizations of US
1192 wildfire and prescribed fire emission ratios and emission factors based on FIREX-AQ aircraft
1193 measurements, *Atmos. Chem. Phys.*, In prep, 2022.

1194 Gueneron, M., Erickson, M. H., VanderSchelden, G. S., and Jobson, B. T.: PTR-MS fragmentation
1195 patterns of gasoline hydrocarbons, *International Journal of Mass Spectrometry*, 379, 97-109,
1196 <https://doi.org/10.1016/j.ijms.2015.01.001>, 2015.

1197 Guenther, A. B., Jiang, X., Heald, C. L., Sakulyanontvittaya, T., Duhl, T., Emmons, L. K., and Wang,
1198 X.: The Model of Emissions of Gases and Aerosols from Nature version 2.1 (MEGAN2.1): an
1199 extended and updated framework for modeling biogenic emissions, *Geosci. Model Dev.*, 5,
1200 1471-1492, 10.5194/gmd-5-1471-2012, 2012.

1201 Herndon, S. C., Jayne, J. T., Zahniser, M. S., Worsnop, D. R., Knighton, B., Alwine, E., Lamb, B. K.,
1202 Zavala, M., Nelson, D. D., McManus, J. B., Shorter, J. H., Canagaratna, M. R., Onasch, T. B., and
1203 Kolb, C. E.: Characterization of urban pollutant emission fluxes and ambient concentration

- 1204 distributions using a mobile laboratory with rapid response instrumentation, *Faraday*
1205 *Discussions*, 130, 327-339, [10.1039/B500411J](https://doi.org/10.1039/B500411J), 2005.
- 1206 Holzinger, R., Acton, W. J. F., Bloss, W. J., Breitenlechner, M., Crilley, L. R., Dusanter, S., Gonin,
1207 M., Gros, V., Keutsch, F. N., Kiendler-Scharr, A., Kramer, L. J., Krechmer, J. E., Languille, B.,
1208 Locoge, N., Lopez-Hilfiker, F., Materić, D., Moreno, S., Nemitz, E., Quéléver, L. L. J., Sarda Esteve,
1209 R., Sauvage, S., Schallhart, S., Sommariva, R., Tillmann, R., Wedel, S., Worton, D. R., Xu, K., and
1210 Zaytsev, A.: Validity and limitations of simple reaction kinetics to calculate concentrations of
1211 organic compounds from ion counts in PTR-MS, *Atmos. Meas. Tech.*, 12, 6193-6208,
1212 [10.5194/amt-12-6193-2019](https://doi.org/10.5194/amt-12-6193-2019), 2019.
- 1213 Inomata, S., and Tanimoto, H.: A deuterium-labeling study on the reproduction of hydronium
1214 ions in the PTR-MS detection of ethanol, *International Journal of Mass Spectrometry*, 285, 95-
1215 99, <https://doi.org/10.1016/j.ijms.2009.05.001>, 2009.
- 1216 Inomata, S., Tanimoto, H., Kato, S., Suthawaree, J., Kanaya, Y., Pochanart, P., Liu, Y., and Wang,
1217 Z.: PTR-MS measurements of non-methane volatile organic compounds during an intensive field
1218 campaign at the summit of Mount Tai, China, in June 2006, *Atmos. Chem. Phys.*, 10, 7085-7099,
1219 [10.5194/acp-10-7085-2010](https://doi.org/10.5194/acp-10-7085-2010), 2010.
- 1220 Jobson, B. T., Alexander, M. L., Maupin, G. D., and Muntean, G. G.: On-line analysis of organic
1221 compounds in diesel exhaust using a proton transfer reaction mass spectrometer (PTR-MS),
1222 *International Journal of Mass Spectrometry*, 245, 78-89,
1223 <https://doi.org/10.1016/j.ijms.2005.05.009>, 2005.
- 1224 Kari, E., Miettinen, P., Yli-Pirilä, P., Virtanen, A., and Faiola, C. L.: PTR-ToF-MS product ion
1225 distributions and humidity-dependence of biogenic volatile organic compounds, *International*
1226 *Journal of Mass Spectrometry*, 430, 87-97, <https://doi.org/10.1016/j.ijms.2018.05.003>, 2018.
- 1227 Karl, T., Hansel, A., Cappellin, L., Kaser, L., Herdinger-Blatt, I., and Jud, W.: Selective
1228 measurements of isoprene and 2-methyl-3-buten-2-ol based on NO⁺ ionization
1229 mass spectrometry, *Atmos. Chem. Phys.*, 12, 11877-11884, [10.5194/acp-12-11877-2012](https://doi.org/10.5194/acp-12-11877-2012), 2012.
- 1230 Karl, T., Striednig, M., Graus, M., Hammerle, A., and Wohlfahrt, G.: Urban flux measurements
1231 reveal a large pool of oxygenated volatile organic compound emissions, *Proc. Natl. Acad. Sci.*
1232 *U.S.A.*, 115, 1186-1191, [10.1073/pnas.1714715115](https://doi.org/10.1073/pnas.1714715115), 2018.
- 1233 Kaser, L., Karl, T., Schnitzhofer, R., Graus, M., Herdinger-Blatt, I. S., DiGangi, J. P., Sive, B.,
1234 Turnipseed, A., Hornbrook, R. S., Zheng, W., Flocke, F. M., Guenther, A., Keutsch, F. N., Apel, E.,
1235 and Hansel, A.: Comparison of different real time VOC measurement techniques in a ponderosa
1236 pine forest, *Atmos. Chem. Phys.*, 13, 2893-2906, [10.5194/acp-13-2893-2013](https://doi.org/10.5194/acp-13-2893-2013), 2013.
- 1237 Khare, P., Machesky, J., Soto, R., He, M., Presto, A. A., and Gentner, D. R.: Asphalt-related
1238 emissions are a major missing nontraditional source of secondary organic aerosol precursors,
1239 *Science Advances*, 6, eabb9785, [doi:10.1126/sciadv.abb9785](https://doi.org/10.1126/sciadv.abb9785), 2020.

1240 Khare, P., Krechmer, J. E., Machesky, J. E., Hass-Mitchell, T., Cao, C., Wang, J., Majluf, F., Lopez-
1241 Hilfiker, F., Malek, S., Wang, W., Seltzer, K., Pye, H. O. T., Commane, R., McDonald, B. C.,
1242 Toledo-Crow, R., Mak, J. E., and Gentner, D. R.: Ammonium adduct chemical ionization to
1243 investigate anthropogenic oxygenated gas-phase organic compounds in urban air, *Atmos.*
1244 *Chem. Phys.*, 22, 14377-14399, 10.5194/acp-22-14377-2022, 2022.

1245 Kilgour, D., Novak, G., and Bertram, T.: Observations of Biotic and Abiotic Marine Volatile
1246 Organic Compounds Emitted from Coastal Seawater, December 01, 2021, 2021.

1247 Kim, S.-W., McDonald, B. C., Seo, S., Kim, K.-M., and Trainer, M.: Understanding the Paths of
1248 Surface Ozone Abatement in the Los Angeles Basin, *Journal of Geophysical Research:*
1249 *Atmospheres*, 127, e2021JD035606, <https://doi.org/10.1029/2021JD035606>, 2022.

1250 Klein, F., Platt, S. M., Farren, N. J., Detournay, A., Bruns, E. A., Bozzetti, C., Daellenbach, K. R.,
1251 Kilic, D., Kumar, N. K., Pieber, S. M., Slowik, J. G., Temime-Roussel, B., Marchand, N., Hamilton,
1252 J. F., Baltensperger, U., Prévôt, A. S. H., and El Haddad, I.: Characterization of Gas-Phase
1253 Organics Using Proton Transfer Reaction Time-of-Flight Mass Spectrometry: Cooking Emissions,
1254 *Environmental Science & Technology*, 50, 1243-1250, 10.1021/acs.est.5b04618, 2016.

1255 Koss, A., Yuan, B., Warneke, C., Gilman, J. B., Lerner, B. M., Veres, P. R., Peischl, J., Eilerman, S.,
1256 Wild, R., Brown, S. S., Thompson, C. R., Ryerson, T., Hanisco, T., Wolfe, G. M., Clair, J. M. S.,
1257 Thayer, M., Keutsch, F. N., Murphy, S., and de Gouw, J.: Observations of VOC emissions and
1258 photochemical products over US oil- and gas-producing regions using high-resolution H₃O⁺
1259 CIMS (PTR-ToF-MS), *Atmos. Meas. Tech.*, 10, 2941-2968, 10.5194/amt-10-2941-2017, 2017.

1260 Koss, A. R., Sekimoto, K., Gilman, J. B., Selimovic, V., Coggon, M. M., Zarzana, K. J., Yuan, B.,
1261 Lerner, B. M., Brown, S. S., Jimenez, J. L., Krechmer, J., Roberts, J. M., Warneke, C., Yokelson, R.
1262 J., and de Gouw, J.: Non-methane organic gas emissions from biomass burning: identification,
1263 quantification, and emission factors from PTR-ToF during the FIREX 2016 laboratory
1264 experiment, *Atmos. Chem. Phys.*, 18, 3299-3319, 10.5194/acp-18-3299-2018, 2018.

1265 Krechmer, J., Lopez-Hilfiker, F., Koss, A., Hutterli, M., Stoermer, C., Deming, B., Kimmel, J.,
1266 Warneke, C., Holzinger, R., Jayne, J., Worsnop, D., Fuhrer, K., Gonin, M., and de Gouw, J.:
1267 Evaluation of a New Reagent-Ion Source and Focusing Ion-Molecule Reactor for Use in Proton-
1268 Transfer-Reaction Mass Spectrometry, *Analytical Chemistry*, 90, 12011-12018,
1269 10.1021/acs.analchem.8b02641, 2018.

1270 Lerner, B. M., Gilman, J. B., Aikin, K. C., Atlas, E. L., Goldan, P. D., Graus, M., Hendershot, R.,
1271 Isaacman-VanWertz, G. A., Koss, A., Kuster, W. C., Lueb, R. A., McLaughlin, R. J., Peischl, J.,
1272 Sueper, D., Ryerson, T. B., Tokarek, T. W., Warneke, C., Yuan, B., and de Gouw, J. A.: An
1273 improved, automated whole air sampler and gas chromatography mass spectrometry analysis
1274 system for volatile organic compounds in the atmosphere, *Atmos. Meas. Tech.*, 10, 291-313,
1275 10.5194/amt-10-291-2017, 2017.

1276 McDonald, B. C., de Gouw, J. A., Gilman, J. B., Jathar, S. H., Akherati, A., Cappa, C. D., Jimenez, J.
1277 L., Lee-Taylor, J., Hayes, P. L., McKeen, S. A., Cui, Y. Y., Kim, S. W., Gentner, D. R., Isaacman-
1278 VanWertz, G., Goldstein, A. H., Harley, R. A., Frost, G. J., Roberts, J. M., Ryerson, T. B., and
1279 Trainer, M.: Volatile chemical products emerging as largest petrochemical source of urban
1280 organic emissions, *Science*, 359, 760-764, 10.1126/science.aag0524, 2018a.

1281 McDonald, B. C., McKeen, S. A., Cui, Y. Y., Ahmadov, R., Kim, S.-W., Frost, G. J., Pollack, I. B.,
1282 Peischl, J., Ryerson, T. B., Holloway, J. S., Graus, M., Warneke, C., Gilman, J. B., de Gouw, J. A.,
1283 Kaiser, J., Keutsch, F. N., Hanisco, T. F., Wolfe, G. M., and Trainer, M.: Modeling Ozone in the
1284 Eastern U.S. using a Fuel-Based Mobile Source Emissions Inventory, *Environmental Science &
1285 Technology*, 52, 7360-7370, 10.1021/acs.est.8b00778, 2018b.

1286 Müller, M., Mikoviny, T., Feil, S., Haidacher, S., Hanel, G., Hartungen, E., Jordan, A., Märk, L.,
1287 Mutschlechner, P., Schotchkowsky, R., Sulzer, P., Crawford, J. H., and Wisthaler, A.: A compact
1288 PTR-ToF-MS instrument for airborne measurements of volatile organic compounds at high
1289 spatiotemporal resolution, *Atmos. Meas. Tech.*, 7, 3763-3772, 10.5194/amt-7-3763-2014, 2014.

1290 Pagonis, D., Sekimoto, K., and de Gouw, J.: A Library of Proton-Transfer Reactions of H₃O⁺ Ions
1291 Used for Trace Gas Detection, *Journal of The American Society for Mass Spectrometry*, 30,
1292 1330-1335, 10.1007/s13361-019-02209-3, 2019.

1293 Peng, Y., Mouat, A. P., Hu, Y., Li, M., McDonald, B. C., and Kaiser, J.: Source appointment of
1294 volatile organic compounds and evaluation of anthropogenic monoterpene emission estimates
1295 in Atlanta, Georgia, *Atmospheric Environment*, 288, 119324,
1296 <https://doi.org/10.1016/j.atmosenv.2022.119324>, 2022.

1297 Pfannerstill, E. Y., Wang, N., Edtbauer, A., Bourtsoukidis, E., Crowley, J. N., Dienhart, D., Eger, P.
1298 G., Ernle, L., Fischer, H., Hottmann, B., Paris, J. D., Stöner, C., Tadic, I., Walter, D., Lelieveld, J.,
1299 and Williams, J.: Shipborne measurements of total OH reactivity around the Arabian Peninsula
1300 and its role in ozone chemistry, *Atmos. Chem. Phys.*, 19, 11501-11523, 10.5194/acp-19-11501-
1301 2019, 2019.

1302 Pfannerstill, E. Y., Arata, C., Zhu, Q., Schulze, B. C., Woods, R., Harkins, C., Schwantes, R. H.,
1303 McDonald, B. C., Seinfeld, J. H., Bucholtz, A., Cohen, R. C., and Goldstein, A. H.: Comparison
1304 between Spatially Resolved Airborne Flux Measurements and Emission Inventories of Volatile
1305 Organic Compounds in Los Angeles, *Environmental Science & Technology*, 57, 15533-15545,
1306 10.1021/acs.est.3c03162, 2023a.

1307 Pfannerstill, E. Y., Arata, C., Zhu, Q., Schulze, B. C., Woods, R., Seinfeld, J. H., Bucholtz, A.,
1308 Cohen, R. C., and Goldstein, A. H.: Volatile organic compound fluxes in the San Joaquin Valley –
1309 spatial distribution, source attribution, and inventory comparison, *EGUsphere*, 2023, 1-42,
1310 10.5194/egusphere-2023-723, 2023b.

1311 Riva, M., Rantala, P., Krechmer, J. E., Peräkylä, O., Zhang, Y., Heikkinen, L., Garmash, O., Yan, C.,
1312 Kulmala, M., Worsnop, D., and Ehn, M.: Evaluating the performance of five different chemical

- 1313 ionization techniques for detecting gaseous oxygenated organic species, *Atmos. Meas. Tech.*,
1314 12, 2403-2421, 10.5194/amt-12-2403-2019, 2019.
- 1315 Rivera-Rios, J. C., Nguyen, T. B., Crouse, J. D., Jud, W., St. Clair, J. M., Mikoviny, T., Gilman, J. B.,
1316 Lerner, B. M., Kaiser, J. B., de Gouw, J., Wisthaler, A., Hansel, A., Wennberg, P. O., Seinfeld, J. H.,
1317 and Keutsch, F. N.: Conversion of hydroperoxides to carbonyls in field and laboratory
1318 instrumentation: Observational bias in diagnosing pristine versus anthropogenically controlled
1319 atmospheric chemistry, *Geophysical Research Letters*, 41, 8645-8651,
1320 <https://doi.org/10.1002/2014GL061919>, 2014.
- 1321 Romano, A., and Hanna, G. B.: Identification and quantification of VOCs by proton transfer
1322 reaction time of flight mass spectrometry: An experimental workflow for the optimization of
1323 specificity, sensitivity, and accuracy, *Journal of Mass Spectrometry*, 53, 287-295,
1324 <https://doi.org/10.1002/jms.4063>, 2018.
- 1325 Ryerson, T. B., Andrews, A. E., Angevine, W. M., Bates, T. S., Brock, C. A., Cairns, B., Cohen, R. C.,
1326 Cooper, O. R., de Gouw, J. A., Fehsenfeld, F. C., Ferrare, R. A., Fischer, M. L., Flagan, R. C.,
1327 Goldstein, A. H., Hair, J. W., Hardesty, R. M., Hostetler, C. A., Jimenez, J. L., Langford, A. O.,
1328 McCauley, E., McKeen, S. A., Molina, L. T., Nenes, A., Oltmans, S. J., Parrish, D. D., Pederson, J.
1329 R., Pierce, R. B., Prather, K., Quinn, P. K., Seinfeld, J. H., Senff, C. J., Sorooshian, A., Stutz, J.,
1330 Surratt, J. D., Trainer, M., Volkamer, R., Williams, E. J., and Wofsy, S. C.: The 2010 California
1331 Research at the Nexus of Air Quality and Climate Change (CalNex) field study, *Journal of*
1332 *Geophysical Research: Atmospheres*, 118, 5830-5866, <https://doi.org/10.1002/jgrd.50331>,
1333 2013.
- 1334 Schauer, J. J., Kleeman, M. J., Cass, G. R., and Simoneit, B. R. T.: Measurement of Emissions from
1335 Air Pollution Sources. 1. C1 through C29 Organic Compounds from Meat Charbroiling,
1336 *Environmental Science & Technology*, 33, 1566-1577, 10.1021/es980076j, 1999.
- 1337 Simpson, I. J., Blake, N. J., Barletta, B., Diskin, G. S., Fuelberg, H. E., Gorham, K., Huey, L. G.,
1338 Meinardi, S., Rowland, F. S., Vay, S. A., Weinheimer, A. J., Yang, M., and Blake, D. R.:
1339 Characterization of trace gases measured over Alberta oil sands mining operations: 76
1340 speciated C₂–C₁₀ volatile organic compounds (VOCs),
1341 CO₂, CH₄, CO, NO₂, NO_y,
1342 O₃ and SO₂, *Atmos. Chem. Phys.*, 10, 11931-11954, 10.5194/acp-10-
1343 11931-2010, 2010.
- 1344 Simpson, I. J., Blake, D. R., Blake, N. J., Meinardi, S., Barletta, B., Hughes, S. C., Fleming, L. T.,
1345 Crawford, J. H., Diskin, G. S., Emmons, L. K., Fried, A., Guo, H., Peterson, D. A., Wisthaler, A.,
1346 Woo, J.-H., Barré, J., Gaubert, B., Kim, J., Kim, M. J., Kim, Y., Knote, C., Mikoviny, T., Pusede, S.
1347 E., Schroeder, J. R., Wang, Y., Wennberg, P. O., and Zeng, L.: Characterization, sources and
1348 reactivity of volatile organic compounds (VOCs) in Seoul and surrounding regions during
1349 KORUS-AQ, *Elementa: Science of the Anthropocene*, 8, 10.1525/elementa.434, 2020.

- 1350 Spanel, P., and Smith, D.: SIFT studies of the reactions of H₃O⁺, NO⁺ and O₂⁺ with a series of
1351 alcohols, *International Journal of Mass Spectrometry and Ion Processes*, 167-168, 375-388,
1352 [https://doi.org/10.1016/S0168-1176\(97\)00085-2](https://doi.org/10.1016/S0168-1176(97)00085-2), 1997.
- 1353 Stark, H., Yatavelli, R. L. N., Thompson, S. L., Kimmel, J. R., Cubison, M. J., Chhabra, P. S.,
1354 Canagaratna, M. R., Jayne, J. T., Worsnop, D. R., and Jimenez, J. L.: Methods to extract
1355 molecular and bulk chemical information from series of complex mass spectra with limited
1356 mass resolution, *International Journal of Mass Spectrometry*, 389, 26-38,
1357 <https://doi.org/10.1016/j.ijms.2015.08.011>, 2015.
- 1358 Stockwell, C. E., Coggon, M. M., Gkatzelis, G. I., Ortega, J., McDonald, B. C., Peischl, J., Aikin, K.,
1359 Gilman, J. B., Trainer, M., and Warneke, C.: Volatile organic compound emissions from solvent-
1360 and water-borne coatings – compositional differences and tracer compound identifications,
1361 *Atmos. Chem. Phys.*, 21, 6005-6022, 10.5194/acp-21-6005-2021, 2021.
- 1362 Tani, A.: Fragmentation and Reaction Rate Constants of Terpenoids Determined by Proton
1363 Transfer Reaction-mass Spectrometry, *Environmental Control in Biology*, 51, 23-29,
1364 10.2525/ecb.51.23, 2013.
- 1365 Tomsche, L., Piel, F., Mikoviny, T., Nielsen, C. J., Guo, H., Campuzano-Jost, P., Nault, B. A.,
1366 Schueneman, M. K., Jimenez, J. L., Halliday, H., Diskin, G., DiGangi, J. P., Nowak, J. B., Wiggins, E.
1367 B., Gargulinski, E., Soja, A. J., and Wisthaler, A.: Measurement report: Emission factors of NH₃
1368 and NH_x for wildfires and agricultural fires in the United States, *Atmos. Chem. Phys.*, 23, 2331-
1369 2343, 10.5194/acp-23-2331-2023, 2023.
- 1370 Vermeuel, M. P., Novak, G. A., Kilgour, D. B., Claflin, M. S., Lerner, B. M., Trowbridge, A. M.,
1371 Thom, J., Cleary, P. A., Desai, A. R., and Bertram, T. H.: Observations of biogenic volatile organic
1372 compounds over a mixed temperate forest during the summer to autumn transition,
1373 *EGUsphere*, 2022, 1-44, 10.5194/egusphere-2022-1015, 2022.
- 1374 Warneke, C., de Gouw, J. A., Kuster, W. C., Goldan, P. D., and Fall, R.: Validation of Atmospheric
1375 VOC Measurements by Proton-Transfer- Reaction Mass Spectrometry Using a Gas-
1376 Chromatographic Preseparation Method, *Environmental Science & Technology*, 37, 2494-2501,
1377 10.1021/es026266i, 2003.
- 1378 Warneke, C., de Gouw, J. A., Holloway, J. S., Peischl, J., Ryerson, T. B., Atlas, E., Blake, D.,
1379 Trainer, M., and Parrish, D. D.: Multiyear trends in volatile organic compounds in Los Angeles,
1380 California: Five decades of decreasing emissions, *J. Geophys. Res.*, 117, 1-10,
1381 10.1029/2012jd017899, 2012.
- 1382 Warneke, C., Geiger, F., Edwards, P. M., Dube, W., Pétron, G., Kofler, J., Zahn, A., Brown, S. S.,
1383 Graus, M., Gilman, J. B., Lerner, B. M., Peischl, J., Ryerson, T. B., de Gouw, J. A., and Roberts, J.
1384 M.: Volatile organic compound emissions from the oil and natural gas industry in the Uintah
1385 Basin, Utah: oil and gas well pad emissions compared to ambient air composition, *Atmos.*
1386 *Chem. Phys.*, 14, 10977-10988, 10.5194/acp-14-10977-2014, 2014.

1387 Warneke, C., Schwarz, J. P., Dibb, J., Kalashnikova, O., Frost, G., Al-Saad, J., Brown, S. S., Brewer,
1388 W. A., Soja, A., Seidel, F. C., Washenfelder, R. A., Wiggins, E. B., Moore, R. H., Anderson, B. E.,
1389 Jordan, C., Yacovitch, T. I., Herndon, S. C., Liu, S., Kuwayama, T., Jaffe, D., Johnston, N.,
1390 Selimovic, V., Yokelson, R., Giles, D. M., Holben, B. N., Goloub, P., Popovici, I., Trainer, M.,
1391 Kumar, A., Pierce, R. B., Fahey, D., Roberts, J., Gargulinski, E. M., Peterson, D. A., Ye, X., Thapa,
1392 L. H., Saide, P. E., Fite, C. H., Holmes, C. D., Wang, S., Coggon, M. M., Decker, Z. C. J., Stockwell,
1393 C. E., Xu, L., Gkatzelis, G., Aikin, K., Lefer, B., Kaspari, J., Griffin, D., Zeng, L., Weber, R., Hastings,
1394 M., Chai, J., Wolfe, G. M., Hanisco, T. F., Liao, J., Campuzano Jost, P., Guo, H., Jimenez, J. L.,
1395 Crawford, J., and Team, T. F.-A. S.: Fire Influence on Regional to Global Environments and Air
1396 Quality (FIREX-AQ), *Journal of Geophysical Research: Atmospheres*, 128, e2022JD037758,
1397 <https://doi.org/10.1029/2022JD037758>, 2023.

1398 Wernis, R. A., Kreisberg, N. M., Weber, R. J., Drozd, G. T., and Goldstein, A. H.: Source
1399 apportionment of VOCs, IVOCs and SVOCs by positive matrix factorization in suburban
1400 Livermore, California, *Atmos. Chem. Phys.*, 22, 14987-15019, 10.5194/acp-22-14987-2022,
1401 2022.

1402 Xu, L., Coggon, M. M., Stockwell, C. E., Gilman, J. B., Robinson, M. A., Breitenlechner, M.,
1403 Lamplugh, A., Crouse, J. D., Wennberg, P. O., Neuman, J. A., Novak, G. A., Veres, P. R., Brown,
1404 S. S., and Warneke, C.: Chemical ionization mass spectrometry utilizing ammonium ions (NH₄⁺
1405 CIMS) for measurements of organic compounds in the atmosphere, *Atmos. Meas. Tech.*, 15,
1406 7353-7373, 10.5194/amt-15-7353-2022, 2022.

1407 Yacovitch, T. I., Herndon, S. C., Pétron, G., Kofler, J., Lyon, D., Zahniser, M. S., and Kolb, C. E.:
1408 Mobile Laboratory Observations of Methane Emissions in the Barnett Shale Region,
1409 *Environmental Science & Technology*, 49, 7889-7895, 10.1021/es506352j, 2015.

1410 Yuan, B., Koss, A., Warneke, C., Gilman, J. B., Lerner, B. M., Stark, H., and de Gouw, J. A.: A high-
1411 resolution time-of-flight chemical ionization mass spectrometer utilizing hydronium ions (H₃O⁺
1412 ToF-CIMS) for measurements of volatile organic compounds in the atmosphere, *Atmos. Meas.*
1413 *Tech.*, 9, 2735-2752, 10.5194/amt-9-2735-2016, 2016.

1414 Yuan, B., Koss, A. R., Warneke, C., Coggon, M., Sekimoto, K., and de Gouw, J. A.: Proton-
1415 Transfer-Reaction Mass Spectrometry: Applications in Atmospheric Sciences, *Chem. Rev.*, 117,
1416 13187-13229, 10.1021/acs.chemrev.7b00325, 2017.

1417